



Lawrence Berkeley Laboratory

UNIVERSITY OF CALIFORNIA

Materials & Molecular Research Division

ELECTROLYTIC GAS EVOLUTION IN FORCED FLOW

Wing Cheong Hui
(M.S. thesis)

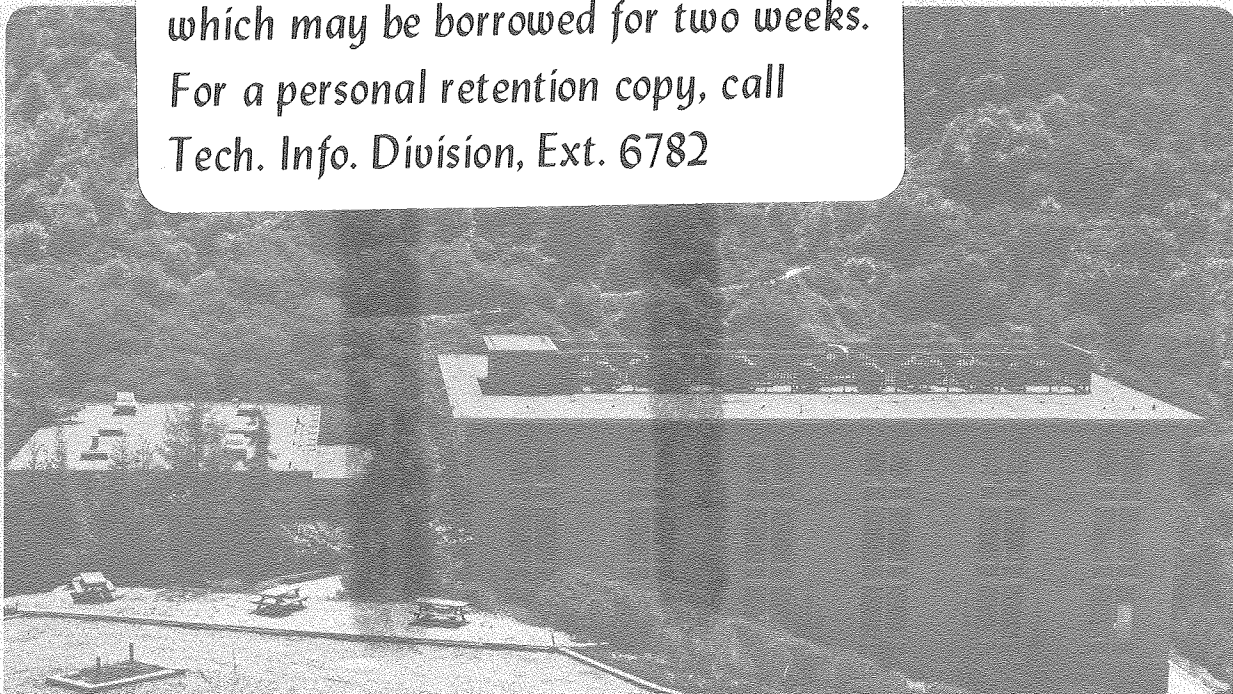
with Charles W. Tobias

December 1980

RECEIVED
BERKELEY LABORATORY
JUN 30 1981
LIBRARY AND
DOCUMENTS SECTION

TWO-WEEK LOAN COPY

*This is a Library Circulating Copy
which may be borrowed for two weeks.
For a personal retention copy, call
Tech. Info. Division, Ext. 6782*



LBL-11945
c. 2

DISCLAIMER

This document was prepared as an account of work sponsored by the United States Government. While this document is believed to contain correct information, neither the United States Government nor any agency thereof, nor the Regents of the University of California, nor any of their employees, makes any warranty, express or implied, or assumes any legal responsibility for the accuracy, completeness, or usefulness of any information, apparatus, product, or process disclosed, or represents that its use would not infringe privately owned rights. Reference herein to any specific commercial product, process, or service by its trade name, trademark, manufacturer, or otherwise, does not necessarily constitute or imply its endorsement, recommendation, or favoring by the United States Government or any agency thereof, or the Regents of the University of California. The views and opinions of authors expressed herein do not necessarily state or reflect those of the United States Government or any agency thereof or the Regents of the University of California.

LEGAL NOTICE

This book was prepared as an account of work sponsored by an agency of the United States Government. Neither the United States Government nor any agency thereof, nor any of their employees, makes any warranty, express or implied, or assumes any legal liability or responsibility for the accuracy, completeness, or usefulness of any information, apparatus, product, or process disclosed, or represents that its use would not infringe privately owned rights. Reference herein to any specific commercial product, process, or service by trade name, trademark, manufacturer, or otherwise, does not necessarily constitute or imply its endorsement, recommendation, or favoring by the United States Government or any agency thereof. The views and opinions of authors expressed herein do not necessarily state or reflect those of the United States Government or any agency thereof.

ELECTROLYTIC GAS EVOLUTION IN FORCED FLOW

Wing Cheong Hui
(M.S. Thesis)

with Charles W. Tobias

Lawrence Berkeley Laboratory
University of California
Berkeley, CA 94720

December 1980

This work was supported by the U.S. Department of Energy
under Contract No. W-7405-ENG-48.

Electrolytic Gas Evolution In Forced Flow

Wing Cheong Hui with Charles W. Tobias

Materials and Molecular Research Division, Lawrence Berkeley Laboratory
and Department of Chemical Engineering; University of California,
Berkeley, California 94720

ABSTRACT

The effects of forced flow and cathode surface morphology on the nature of hydrogen bubble evolution in 5M KOH solution have been investigated in a flow system; a special flow channel allowed both optical observation and electrical measurement to be carried out simultaneously. Optical observation was made with regular- and high- speed cameras. Both the overpotential and the incremental ohmic drop caused by bubbles were determined over the current density range of 0.4 - 2,000 mA/cm² for purposes of engineering analysis.

The bubble evolution behavior was found to depend strongly on the surface morphology of the electrode. This behavior is dominated by the density and the distribution of nucleation sites. Both the bubble size and the incremental resistance caused by bubbles increase with increasing current density. The incremental resistance ranges from a few tenths of an ohm to 2.5 Ω depending on the surface morphology. The corresponding incremental ohmic drop changes from several mV to a few hundred mV, depending on the current density. While forced flow reduces the mass transfer resistance appreciably only at low current densities (< 10 mA/cm²), it may decrease the incremental ohmic drop at current densities above 40 mA/cm² by as much as 30-55 %.

(I) INTRODUCTION

Gas evolution by electrolysis occurs in many common electro-synthetic processes in industry. For example, the production of hydrogen, chlorine and caustic soda by the electrolysis of brine, and the production of hydrogen and oxygen by the electrolysis of water are widely employed. The electrolysis of brine is not only one of the oldest, but also one of the most important industrial electrochemical processes. Today, the free world produces about 30 million tons of chlorine each year¹; and at least 96% of it is produced by the electrolysis of brine². Although the water electrolysis industry is not as large as the chlor-alkali industry, it has also become an important process since the beginning of this century. The United States alone produces at least 250,000 tons of high purity hydrogen by electrolysis each year³.

For gas synthesis, the electrolytic methods certainly have several intrinsic advantages over others: high purity gases are readily produced, the equipment can be made fully automatic, and considerable flexibility of output is possible. Usually, the economics of these processes depends largely on the cost of electrical power. Therefore, water electrolysis is used only when high purity of gas is desired or cheap electrical power is available. However, over the last three decades, nuclear energy has grown from an exciting experimental stage to the point where it can produce a significant fraction of the world's electrical energy supply. This accomplishment certainly will make the cost of electricity relatively lower; and thus electrolytic processes will become economically more attractive.

With the advent of energy crisis, scientists increasingly look for various alternative energy sources. These include nuclear power, solar energy, synthetic fuel, hydro-electric power, and so on. Water electrolysis has been considered as an intermediate process in converting, storing or transmitting energy in some of these power systems. Proposed scenarios include to produce cheap hydrogen from nuclear energy for the synthesis of liquid and gaseous fuels⁴, to collect and store solar energy by the photoelectrolysis of water⁵, and to store off-peak power from nuclear or hydro-electric power plants^{6,7}. The main advantages of storing energy by the electrolysis of water are that only hydrogen must be stored, and it can be either used directly as a fuel or converted back to electricity simply by a fuel cell in combination with oxygen from the air.

The prospects of producing hydrogen as a supplementary fuel, as a chemical feedstock, or as an intermediate in energy storage are determined by economic considerations, which in turn depend highly on the cell energy efficiency. The power required to run the process is the product of the cell voltage and the current, $P = VI$. The cell voltage comprises the reversible potential, the anodic and cathodic overpotentials, and the ohmic losses. The ohmic drop arises mainly from two sources: from the diaphragm and from the electrolyte itself. The resistance of the electrolyte depends on both its conductivity and the void fraction of the gas bubbles. Many attempts have been made to decrease the overpotentials by using various types of electrode geometries and to reduce the IR-drop by trying new types of diaphragms. Others have tried to increase the efficiency by raising the electrolyte temperature and/or the system pressure⁸. With the increase in electrolyte temperature, the reversible voltage, the overpotentials, and the resistivity of the electrolyte decreases simultaneously. Increasing the system pressure will raise the reversible potential. This effect, however, will be offset by the reduction of the IR-drop of the electrolyte due to the smaller bubble void fraction. Above and beyond all these methods, another way to reduce the electrolyte ohmic drop is by using forced convection⁹⁻¹². This in fact is the main interest of our project : to study how the incremental resistance caused by bubbles will be decreased by forced flow and by various surface finishes of the electrode.

Literature Review

Detailed literature reviews on earlier studies of gas evolution have been given by Ronald Alan Putt¹³, and A.T.Kuhn, J.Bin Yusof and P. Hogan¹⁴. Here, we attempt to review only the literature that is directly related to our work. The major interest in our study is to investigate the effects of forced flow and surface morphology of electrode on the gas evolution behavior by means of optical observation and electrical measurements (such as overpotential and resistance measurements).

Putt¹³ investigated the events associated with the evolution of hydrogen and oxygen at

the electrode surface in concentrated sulfuric acid and KOH solutions. Bubble growth rate, number density, and maximum bubble size data were obtained at current densities of 500-2000 mA/cm² at the incipient bubble growth stage. The growth characteristics of the bubbles were found to depend strongly on electrolyte composition. They are different for hydrogen and oxygen electrodes in the same electrolyte. In sulfuric acid solution, larger hydrogen bubbles are formed at the cathode, and smaller oxygen bubbles at the anode. In KOH solution, the trend is reversed---smaller hydrogen bubbles at the cathode and bigger oxygen bubbles at the anode. Within the range studied, increasing the gas generation rate does not change the character of the events. It only influences the rate of their occurrence. Usually, repeated sequences of coalescence are involved in the bubble growth before separation from the electrode. Putt had also claimed that the microscopic roughness of a planar electrode had little effect on the character of gas evolution.

A hydrodynamic study of the bubble effects on the IR-drops in a vertical rectangular cell was carried out by F. Hine, M. Yasuda, R. Nakamura, and T. Noda¹¹. They evolved hydrogen gas on a 304 stainless steel cathode in 1.75N sodium hydroxide solution. The resistivity of electrolyte containing hydrogen bubbles was found to increase with the current density, decrease with the operation temperature, and decrease with the flow rate. Naturally, the geometry of the channel also influenced the ohmic drop.

In a similar study, F. Hine and K. Murakami¹² used an electrode divided into 10 segments to obtain the current distribution from the bottom to the top of the cell. The local current density was found to decrease with increasing elevation because of the increasing gas void fraction along the electrode. Hine et al also concluded that the superficial resistivity of the solution containing gas bubbles agrees well with the Bruggeman equation:

$$\rho/\rho_0 = (1 - \epsilon)^{-3/2} \quad (1)$$

where ρ = resistivity of gas-solution mixture, ρ_0 = resistivity of bubble-free solution, and ϵ = gas void fraction. The void fraction and the resistivity ρ can be decreased by means of solution circulation. Also, the anode-to-cathode gap is most important in determining the solution IR-drop; the gas void fraction decreases with increasing gap width but the solution resistance

increases as the width increases. Thus, in agreement with the theoretical treatment advanced by Tobias¹⁵, there is an optimum gap width for each cell design.

Huhn, Yusof and Hogan¹⁴ have investigated the role of electrode structure and surface texture in the performance of gas evolving electrodes. Cell voltage was measured for an undivided cell in 5M NaOH solution at 70°C. In their system, the cathode was either a mild steel plate, mild steel mesh or combinations of these materials. The anode was Ni-plate mild steel sheet or mesh. They found that substantial voltage reduction could be obtained by using multiplex electrode structures and that these are mainly explicable in terms of increased specific surface area. Sheet electrodes seem to be more efficient than mesh ones on this basis. However, it was shown that sheet electrodes with very high specific surface areas demonstrated significantly higher overvoltages than electrodes with low specific area. This surprising result may be explained by bubble entrapment.

(II) EXPERIMENTAL

In the present study, the main objective was to examine the effects of forced flow and surface morphology of the cathode on the hydrogen evolution behavior in KOH solution, as a function of current density. For a detailed study of these effects, a wider range of current density (0.4 to 2,000 mA/cm²) was used than in previous experimental work. Usually, in industrial water electrolysis, the practical range is around 100 to 500 mA/cm².

In regard to the effect of surface morphology, the expectation is not only that the specific surface area will have an effect, but also that the relative distribution of active nucleation sites can have a major influence. Therefore, instead of using mesh type electrodes, cathodes were specially sanded or cut by mechanical means. This allows better control of the nucleation site distribution and of the current density distribution.

Another goal of this project was to obtain a correlation between the incremental resistance caused by bubbles and the bubble size. A special vertical flow channel was constructed such that both optical observations and electrical measurements could be made simultaneously.

(1) Flow System

One of the objectives of this study was to investigate the gas bubble evolution behavior under forced convection. For this purpose, a flow system was constructed. The apparatus is shown photographically in Figure (1) and depicted schematically in Figure (2). Basically, it consists of 3 parts: the flow channel, the reservoir and the flow control system. All the tubing in the system was made of 304 stainless steel. The valves and the fittings were made of 316 stainless steel or Type I PVC. These materials were chosen such that no chemical reaction would occur between the electrolyte and the system. Bleed lines were included for the purpose of cleaning and re-filling.

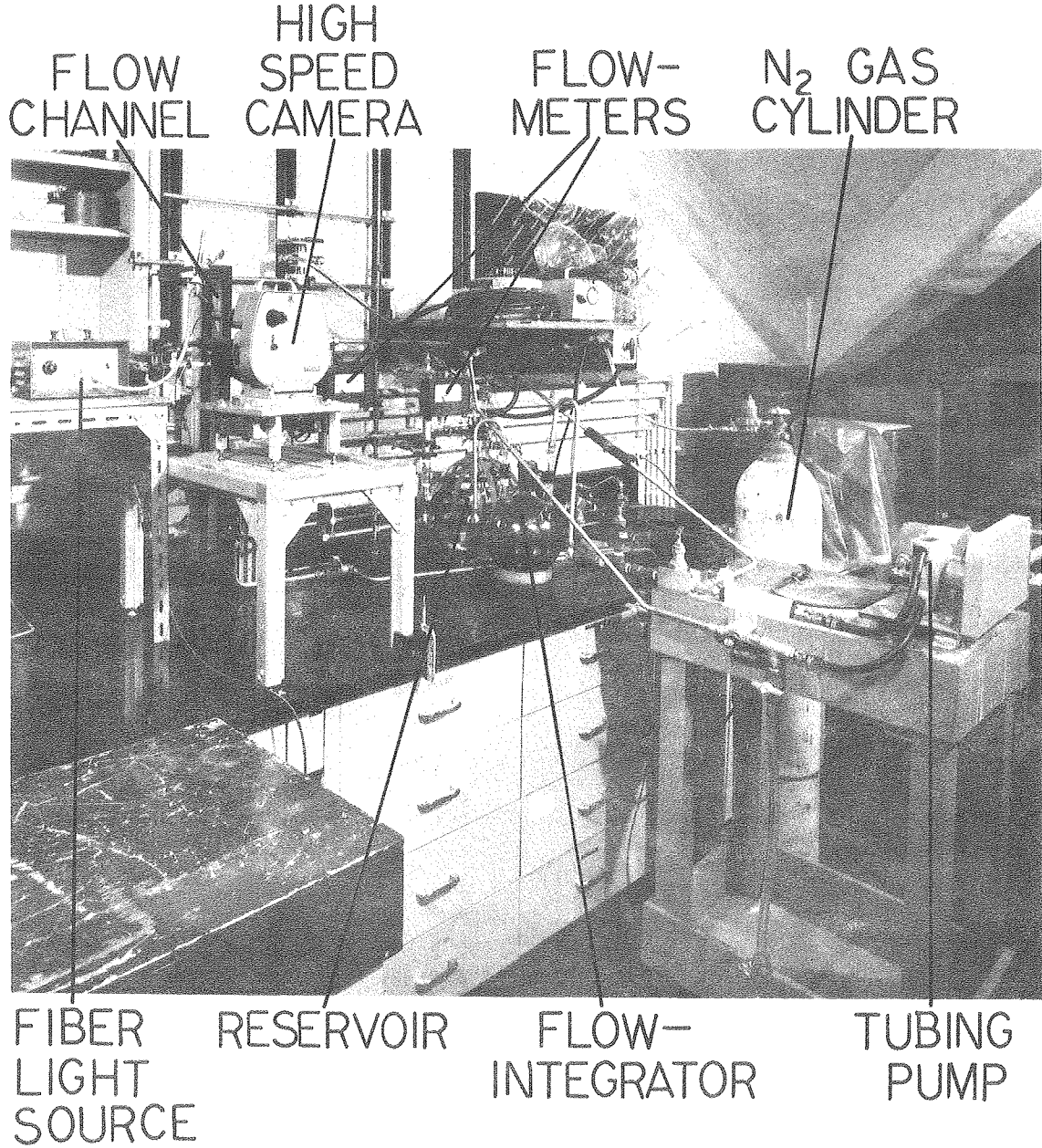


FIGURE (1) PHOTOGRAPH OF THE EXPERIMENTAL APPARATUS

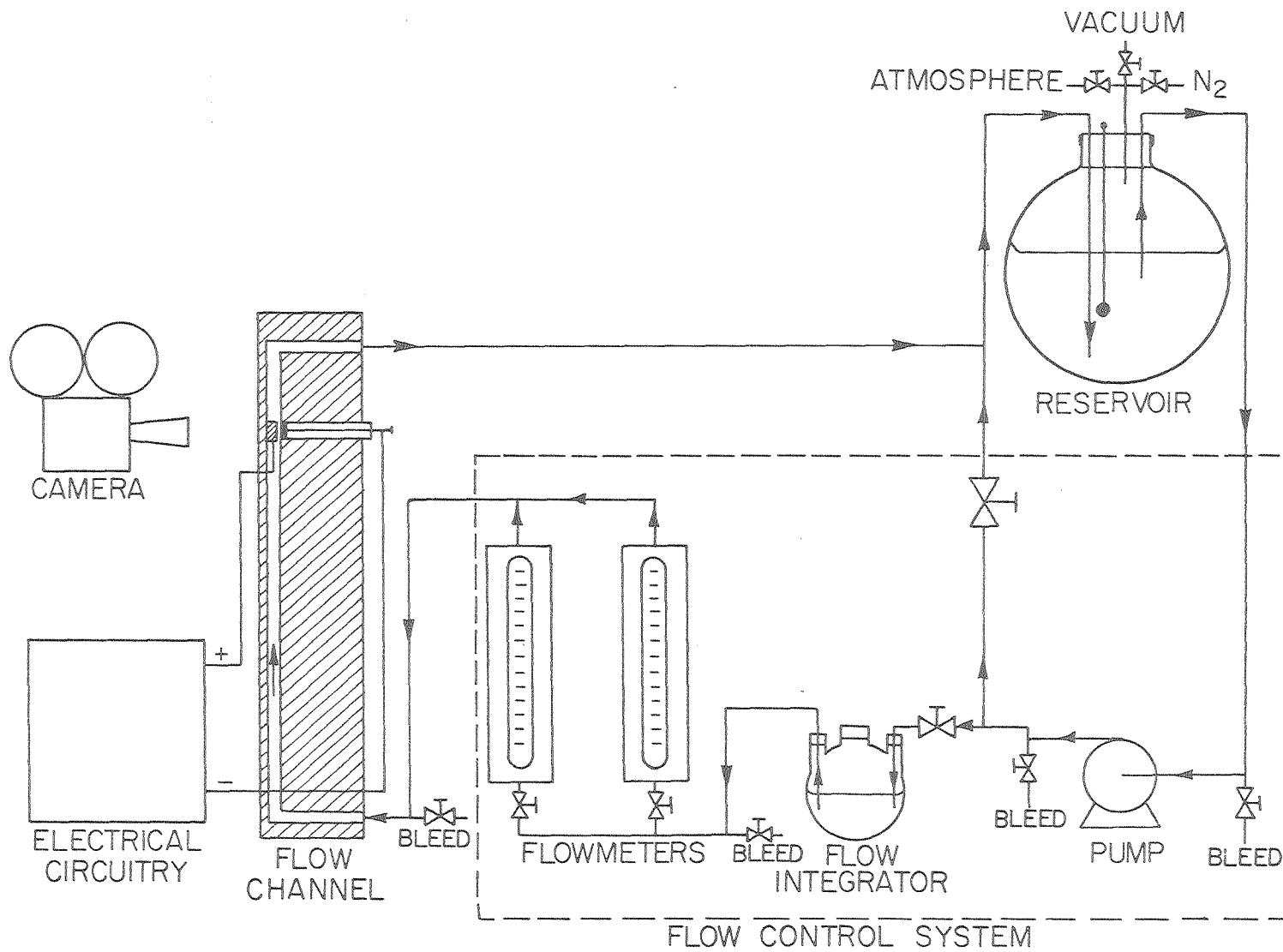


FIGURE (2) FLOW CHART OF THE APPARATUS

XBL804-5049

(i) Flow Channel

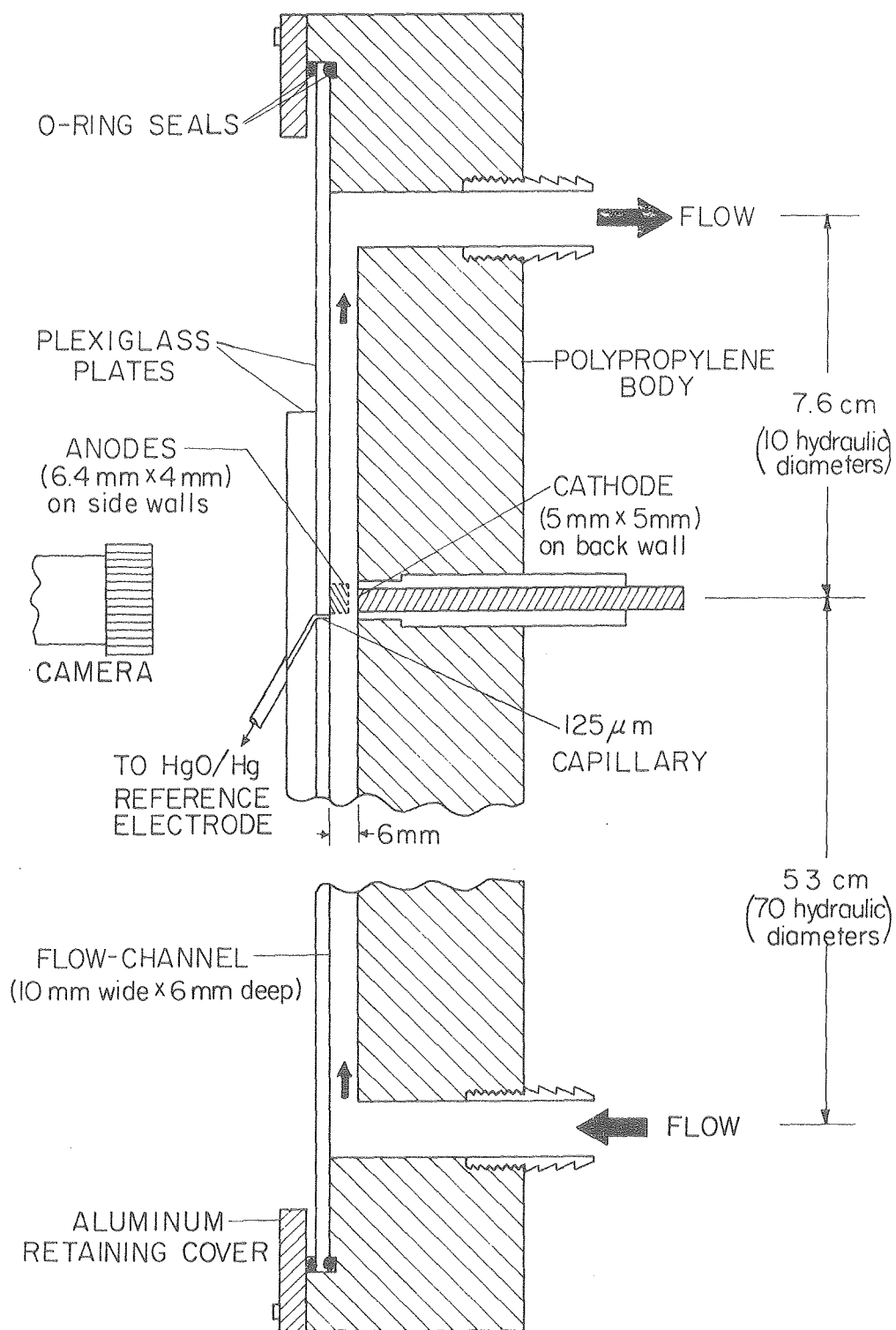
A flow channel designed and constructed by Hellyar¹⁶ was modified for the purposes of this study. The channel body was machined from a single block of polypropylene with overall dimensions of 7.6 cm wide, 4.8 cm deep, and 71.0 cm long. The flow channel itself was milled as a slot into this body. It was 10 mm wide and 6 mm deep. Figure (3) shows a longitudinal cross-section of this flow channel.

Electrolyte was pumped into the channel via a fitting at the lower back end of the cell body. It then flowed up the channel and exited at the rear. The length from the entrance to the electrode region was 53 cm (70 hydraulic diameters), and the length from the electrode to the exit was 7.6 cm (10 hydraulic diameters). With this arrangement, the hydrodynamics in the electrode region should not be influenced by the end effects.

To be able to see and photograph the electrodes, a 1/8" plexiglas plate was mounted on the cell body with an aluminum cover plate. O-rings were mounted in the front and the back of the plexiglas plate to make the channel air-tight.

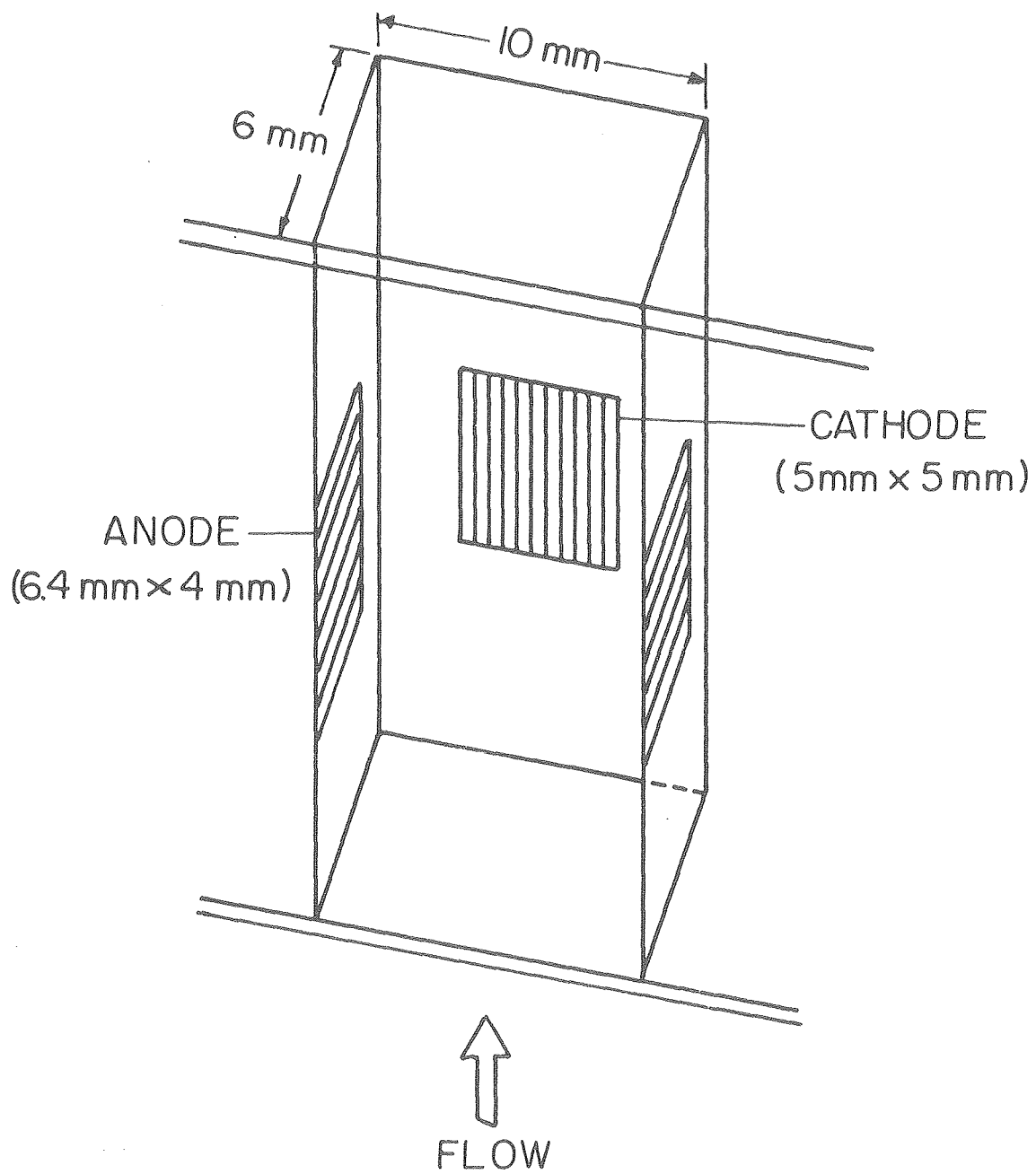
This flow channel differed from Hellyar's in two ways. First, the positions of the cathode and the anode were inter-changed, i.e. the nickel cathode in our cell was placed on the back wall while the two stainless steel anodes were put on the side walls. (See Figure (4).) According to Hellyar's study, this arrangement of electrodes should provide a quite even current distribution on the cathode. The current density should be only slightly higher along the nickel-epoxy edges.

Secondly, a capillary junction was made on the front plexiglas panel for taking overpotential measurements. See Figure (3). For ease of construction, a piece of 1/4" thick plexiglas plate was glued onto the 1/8" plexiglas front panel with acrylic cement. The thicker viewport was still transparent. A 125 μm diameter, 2 mm long hole was then drilled perpendicularly into the back of the viewport. This hole was at a position about 1 mm ahead of the leading edge of the cathode. A bigger hole, about 250 μm in diameter, was then drilled from the front side at 60° from the normal to intersect the 125 μm hole. A 1/4" plexiglas tube was glued onto the



XBL 804-5050

FIGURE (3) SCHEME FOR THE LONGITUDINAL CROSS-SECTION OF THE FLOW CHANNEL



XBL804-5046

FIGURE (4) THE ARRANGEMENT OF THE ELECTRODES IN THE FLOW CHANNEL

opening of this second hole to connect the capillary to a $\text{Hg}/\text{HgO}, \text{OH}^-$ reference electrode. Since the capillary hole was quite far from the cathode, the overpotential measured should be a reasonable average value. This special capillary arrangement allowed simultaneous direct optical observation and overpotential measurement. Figure (5) shows a front view photo of this arrangement.

(ii) Flow Control System

Basically, the flow control system contained four elements: (a) a pump, (b) a recycle line, (c) a flow-integrator, and (d) flow-meters. The electrolyte was pumped by a tubing pump running at a fixed speed. An adjustable recycle line was used to adjust the flow rate. Then the main stream was passed through a flow-integrator to smooth out the pulsation caused by the pump. The flow rate was measured by two flow-meters just before the flow channel. In our experiment, the flow velocity ranged from 40 to 135 cm/sec., which corresponds to Reynolds Number of 2,000 to 6,600, in the low turbulent range.

(a) Pump

The pump employed was a LG-301 Tubing Pump manufactured by the Little Giant Pump Company. Since this pump had a fixed speed of 575 R.P.M., its pumping capacity depended only on the tubing size. With a $3/8" \times 5/8"$ tubing, it could deliver 2.8 G.P.M.; whereas with a $1/2" \times 3/4"$ tubing, its capacity was increased to 4.8 G.P.M. The tubing used for this pump was made of neoprene. This material is reported to be very stable in the 5M KOH solution. To reduce vibration in the system, the pump was installed on a separate table away from the equipment bench.

(b) Recycle Line

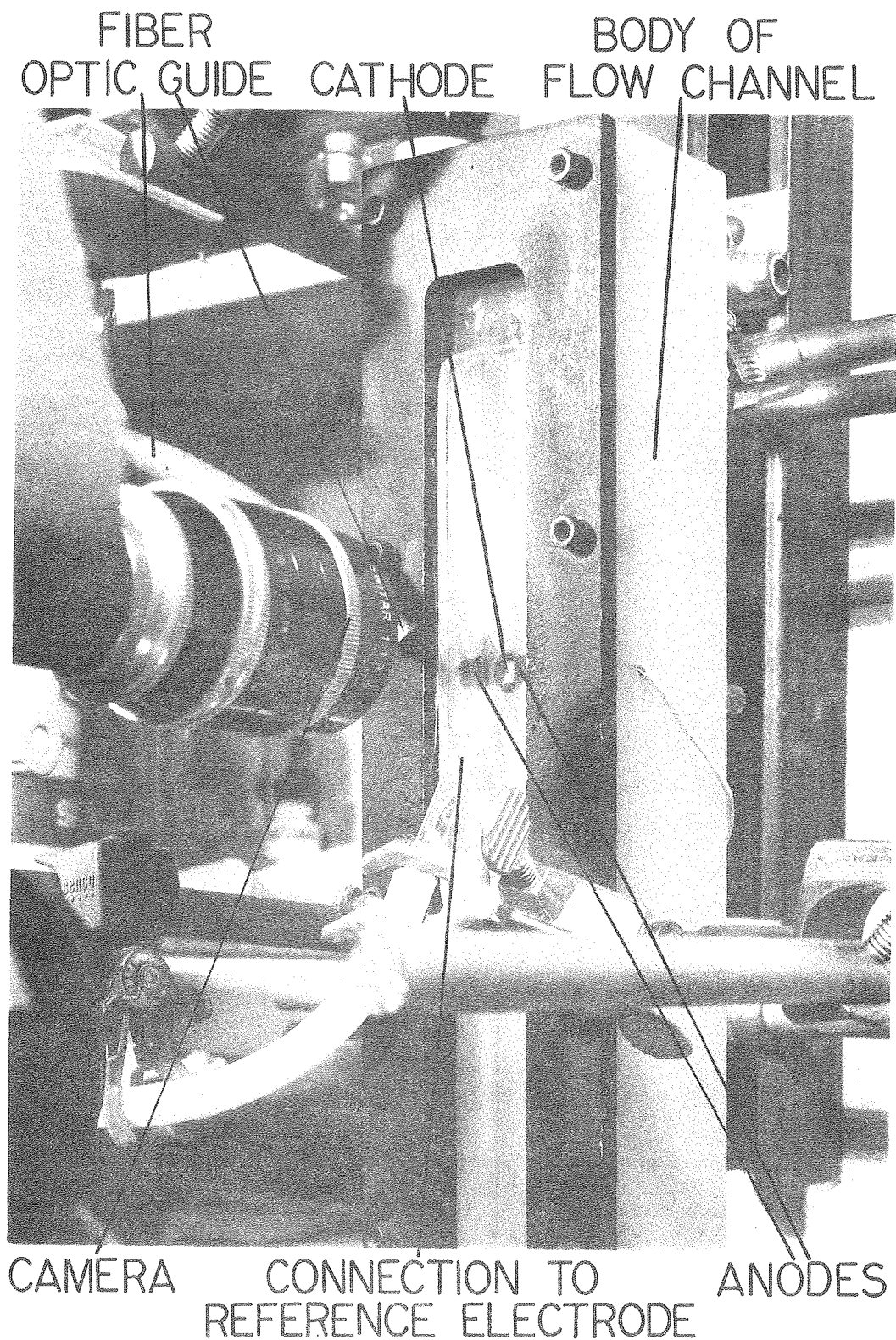


FIGURE (5) A FRONT VIEW PHOTOGRAPH
OF THE FLOW CHANNEL

The recycle line was made of 1/2" 304 stainless steel tubing and an adjustable 1/2" valve made of 316 stainless steel.

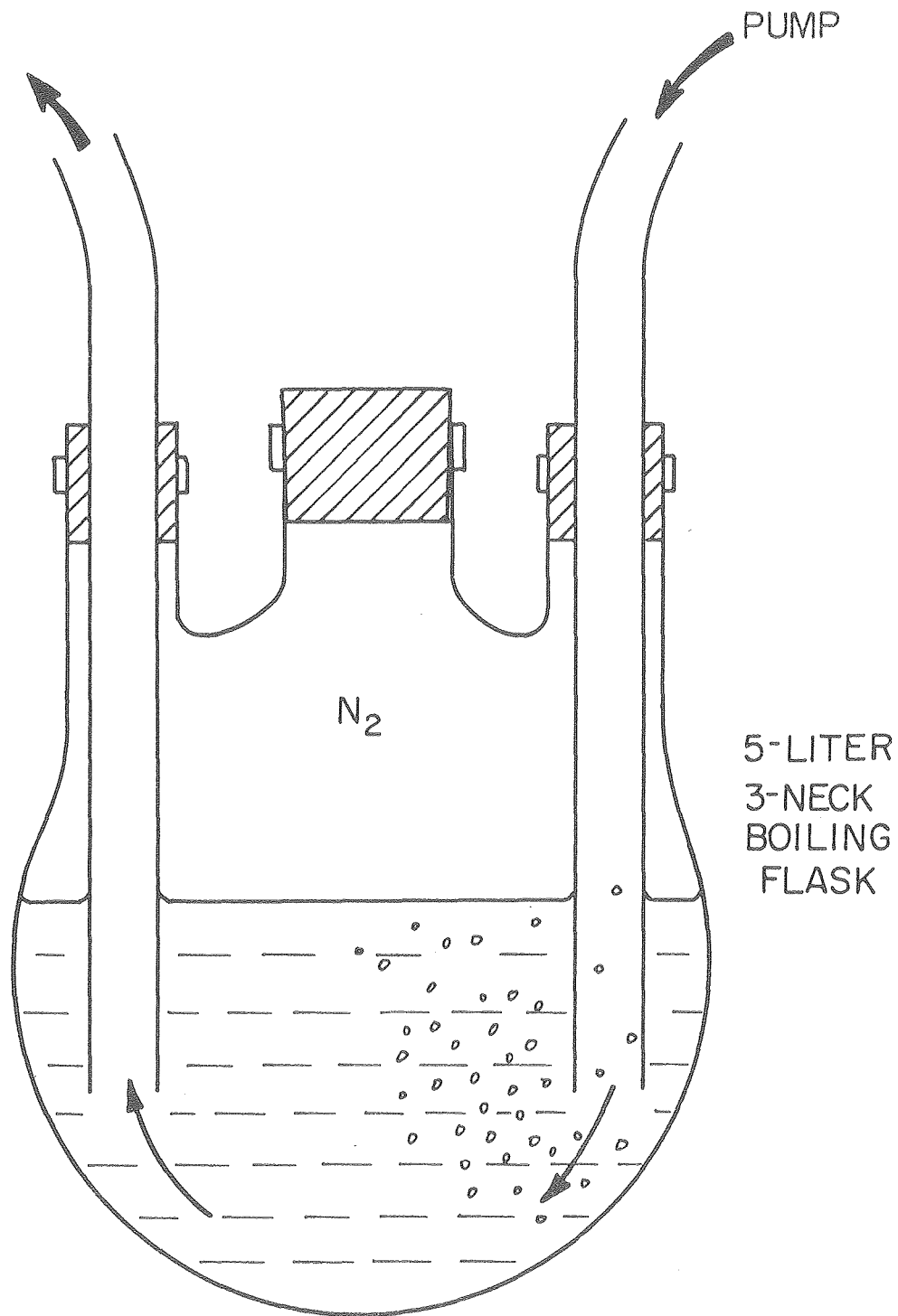
(c) Flow-Integrator

Since tubing pumps have pulsatory outputs, a flow-integrator was constructed to even the flow. A 5-liter three neck Pyrex boiling flask was used. (See Figure (6).) Two glass tubes were run in the flask via the 2 side necks to within about 2" above the bottom. The center neck, used for cleaning purposes, was sealed during operation. The flask was filled with an inert atmosphere of nitrogen. As the electrolyte was being pumped into the flask, the nitrogen atmosphere was compressed, and the electrolyte level would rise to cover the glass tubing ends. With each pulse, the inlet pressure would be increased, the nitrogen atmosphere would be compressed and part of the flow would be "absorbed" in the integrator. In between pulses where inlet pressure dropped, the compressed nitrogen atmosphere would expand to "release" some of the electrolyte into the outlet stream. This flow integrator had been shown to work very well by experience as it could even the flow to a great extent. Another advantage of using this flow integrator is that tiny bubbles carried in the inlet stream could be eliminated from the electrolyte into the flask, making the outlet flow bubble-free.

(d) Flow-Meters

Two Fischer & Porter 10A2227A Dial Flow Indicators were used. They had capacity ranges of 0 to 25 GPH and 0 to 5 GPM of water, respectively. Since 5M KOH solution and water have different densities and viscosities, a correction factor of 1/1.105 was used to correct the flow readout for the 5M KOH solution. The flowmeters were constructed out of 316 stainless steel.

(iii) Reservoir



5-LITER
3-NECK
BOILING
FLASK

XBL 804 - 5 047

FIGURE (6) FLOW INTEGRATOR

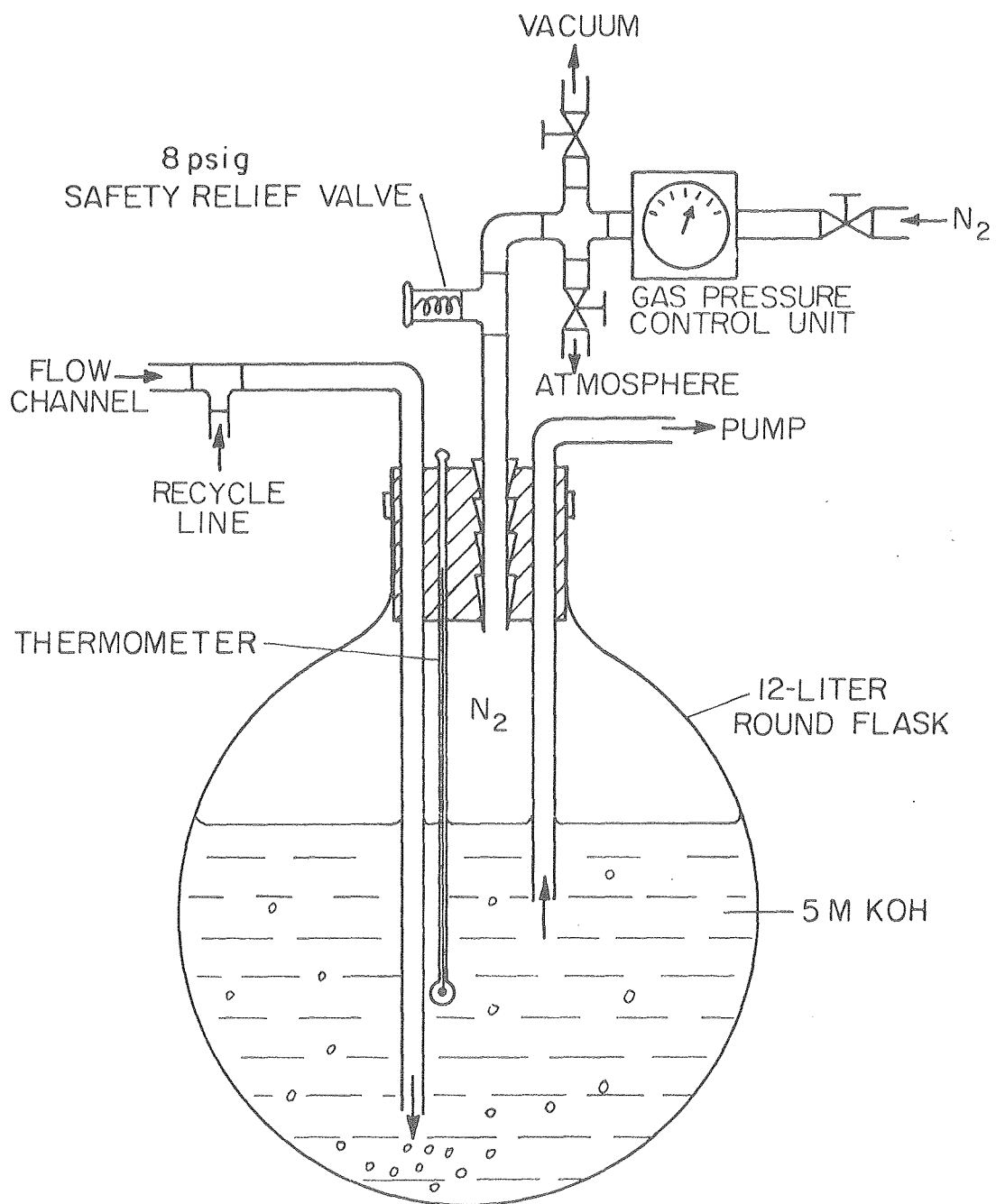
The reservoir was a 12-liter round Pyrex flask. (See Figure (7).) Both the inlet and the outlet were made with 1/2" glass tubes. The inlet tube was made longer than the outlet one to eliminate entrainment of bubbles by the inlet flow. The entire flask was sealed and filled with an inert atmosphere of nitrogen to prevent impurities in the air, particularly carbon dioxide, from contaminating the electrolyte. The flask was connected to a nitrogen gas cylinder, a vacuum system, and the atmosphere. The connection to the atmosphere was used only for balancing pressure during the cleaning and refilling process. During experiments, the vacuum system was always turned on to purge the hydrogen and the oxygen formed by electrolysis. To maintain the reservoir at atmospheric pressure, nitrogen was bled into the flask through a pressure regulator. For the sake of safety, a 8 psig relief valve was installed on the gas line. A thermometer was also put in the flask. All experiments were usually performed at room temperature of 25°C.

(2) Electrolysis System

(i) Electrolyte

In the industrial water electrolysis, 25-35% w/v KOH is commonly used. This electrolyte has the advantage of high conductivity. In this study, 5M KOH (28%) was chosen as the electrolyte. The conductivity of this solution, at 25°C, was measured to be 0.588/ Ω -cm by means of an Impedance Bridge 290A system with a A.C. Generator Detector 861A (by Electro Scientific Industries). The density and the viscosity of this solution at 25°C were 1.191 gm/cc and 1.83 cP respectively.

This electrolyte was prepared with analytical reagent grade potassium hydroxide pellets supplied by Mallinckrodt, Inc. The distilled water used had been treated with a Cartridge-Treatment System manufactured by Culligan. This system contained a deionizer, an organics



XBL 804-5048

FIGURE (7) RESERVOIR

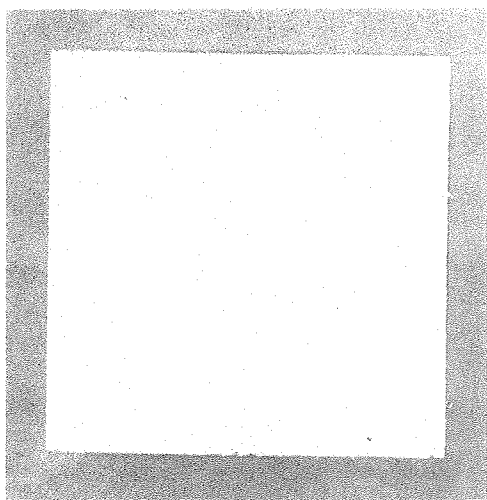
trap and a microfilter. The specific resistance of the treated water was typically larger than 10 Megohm-cm.

(ii) Cathode

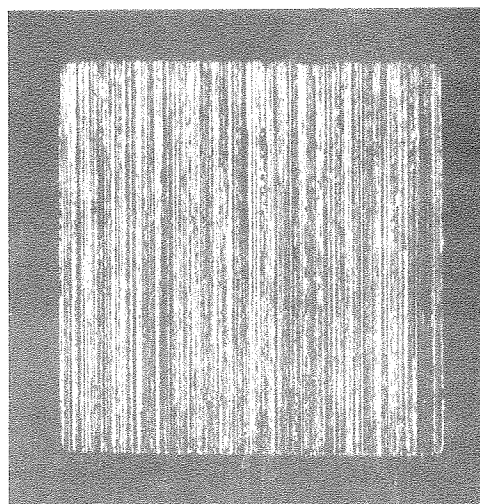
The cathodes were machined from Nickel 200 (99.5% pure Nickel). All the cathodes were 5 mm × 5 mm square. They were cast in machinery epoxy, and attached to the back wall of a vertical flow channel. For the arrangement of the cathode and the anodes, see Figure (4).

Since one of our interests was the effect of the surface morphology of the cathode on bubble formation, several cathodes were used :-

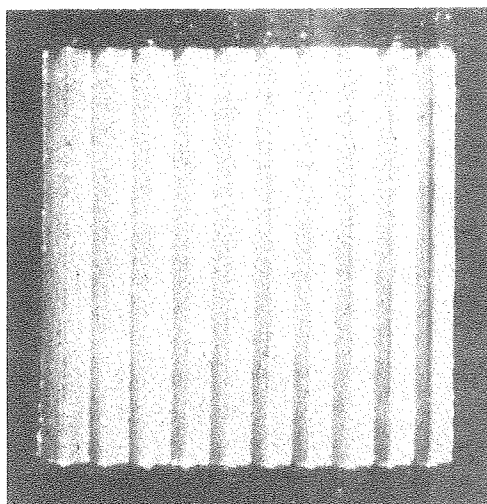
- (a) **Polished Electrode**---The electrode was polished with 1 μm diamond paste with Automat Lapping Oil on a nylon polishing cloth. It was then finished on a Microcloth polishing cloth with water. All these polishing materials were supplied by Buehler Ltd. Figure (8A) shows a magnified photograph (15 \times) of this electrode.
- (b) **Parallel Sanded Electrode**----The electrode was sanded with 100 grit sandpaper. A magnified photo of this surface is shown in Figure (8B). The average groove size is approximately 25.6 μm (0.0001 in.). The electrode was oriented with the sanding lines parallel to the flow.
- (c) **Crosswise Sanded Electrode**----It was exactly the same as Sanded Electrode (1) except with the sanding lines perpendicular to the flow.
- (d) **Parallel Grooved Electrode**----The electrode was cut mechanically with a 60° cutter. As shown in Figure (8C), ten 0.5 mm wide grooves were cut in the 5 mm × 5 mm square. By this grooving, the actual surface area of the electrode was increased from 25 to 50 mm^2 . However, in order to make the electrodes comparable, all the current density calculations were based on the projected area----25 mm^2 . Experiments were carried out with the grooves parallel to the flow.



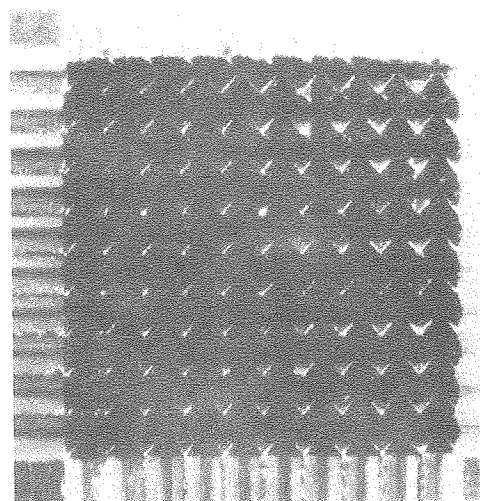
(A) POLISHED ELECTRODE



(B) SANDED ELECTRODE



(C) GROOVED ELECTRODE



(D) PYRAMIDAL ELECTRODE

FIGURE (8) MAGNIFIED PHOTOGRAPHS OF THE CATHODES. THE ACTUAL DIMENSIONS OF THEM ARE 5mm X 5mm.

- (e) **Crosswise Grooved Electrode**----This was exactly the same as Grooved Electrode (1) except with the grooves perpendicular to the flow.
- (f) **Pyramidal Electrode**----This electrode was made by cutting two identical sets of grooves perpendicular to each other on the electrode surface. With this special feature, the total actual surface area also became 50 mm^2 . A photo of it is shown in Figure (8D).

After all the surfaces were finished, the electrodes were cleaned with Latone glass cleaner, water, acetone, Amway Regular Liquid Organic Cleaner, and finally deionized water in sequence. For better reproducibility, each electrode was pre-polarized anodically in 5M KOH at 1 mA/cm for about 10 minutes. Then the current was turned on at the value set for the experiment for 5 minutes before data were taken.

(iii) Anode

There were two 316 stainless steel anodes in the flow cell, each 6.4 mm long and 4 mm wide. They were placed on the 2 side-walls of the flow channel. See Figure (4) for the arrangement of the electrodes.

(3) Optical Systems

One main objective of this study was to make optical observation on the bubble evolution behavior at the cathode. Since the phenomena were too fast for human eyes to follow, specially equipped movie cameras were used to obtain slow motion of the events for purposes of analysis. With proper combinations of lenses and extension tubes, magnified pictures could be obtained. These pictures could be further magnified to any desired size by proper adjustment in

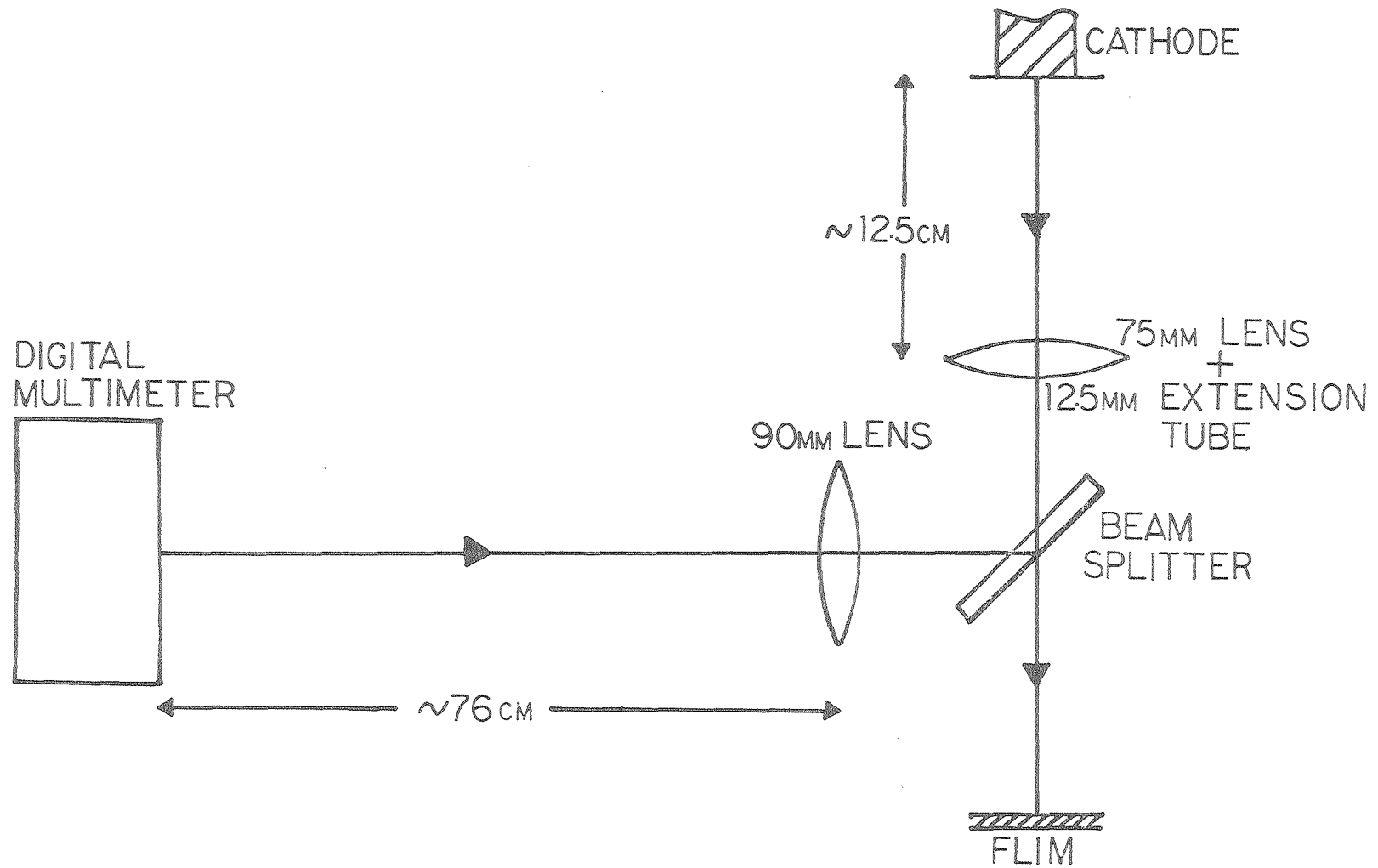
projection. Thus optical analysis could be made more easily.

Usually, at low current densities ($< 20 \text{ mA/cm}^2$) in stagnant electrolyte, the evolution of gas was quite slow. A regular Bolex H16 Movie Camera was therefore used. This camera had filming speeds ranging from 12 to 64 frames/sec. In part of the runs, a beam splitter was employed to make simultaneous superposition of the bubble image and the digital image of a multimeter on the film. An example of this kind of arrangement is illustrated in Figure (9). This special technique was limited to slow filming only (≤ 64 frames/sec), because of the weak light intensity of the light emitting diodes.

At higher current densities, and in flowing electrolyte, a HYCAM Movie Camera made by Red Lake Laboratory was used to catch the faster motions. This camera was capable of taking movies from 200 frames/sec to 10,000 frames/sec. Usually, most movies were taken within 7,000 frames/sec because of limited illumination. Due to our cell construction, only reflected lighting, rather than direct lighting, could be used. (Reflected lighting means the light is directed to the object and reflected to the camera; whereas direct lighting means the light is shined directly through the object into the camera.) This range of speed was high enough for most of the events studied. However, the image superposition technique cannot be used in the high speed filming range. Nevertheless, a recording of the electrical measurements by the side of the film worked out as well, because the voltage readings were quite stable throughout each run.

High intensity illumination for the movies were obtained by using the 22-0004 Fibre Light Source and the Fibre Optic Guides supplied by Ealing Optic Corp. A 150 W Tungsten filament lamp was used for the light source. Usually, the radiance output from a 2 ft long fibre optic guide was around 2800 mW/cm^2 for 100% voltage input, or 770 mW/cm^2 for 75% voltage input.

Either Kodak 7278 Tri-X (ASA 200) or Kodak 7277 4-X (ASA 400) Reversal Black and White Film (100 ft roll) was used. Since the film length was limited, filming speed had to be adjusted so that the movie taken was long enough to study all sequences and fast enough to catch the detail of each sequence.



XBL 805-9696

FIGURE (9) AN EXAMPLE OF THE TECHNIQUE FOR SUPERPOSITION OF IMAGES BY MEANS OF A BEAM SPLITTER.

(4) Electrical Equipments & Measurements

In our study, all experiments were run galvanostatically. The power supply used was an Amel Model 551 Potentiostat-Galvanostat manufactured by EOC-Control, Inc. With this equipment, current densities could be ranged from 0.4 mA/cm^2 up to 2 A/cm^2 for cathodes of 0.25 cm^2 . For the information of voltage requirement, electrical circuit was set up to make overpotential and ohmic drop measurements.

(i) Overpotential Measurement

As mentioned in Section (II) (2) (ii), a Hg/HgO,OH^- reference electrode was connected to the flow cell through a capillary junction for overpotential measurements. This kind of reference electrode is supposed to have a relatively long life, and should be reproducible to better than $\pm 0.1 \text{ mV}^{17}$. By experience, this reference electrode was found to stay stable for longer than two weeks in our system. Its standard electrode potential, referred to the hydrogen electrode, is 0.098 V . Overpotential measurements was made by using either a Keithley 72A Digital Multimeter or a Nicolet 1090A EXPLORER Digital Oscilloscope. The voltage measured was primarily the sum of three terms : the overpotential of the cathode, the standard potential difference between the cathode and the reference electrode, and the ohmic drop from the capillary tip to the cathode surface. The standard potential difference is 0.926 V . The ohmic drop could be determined by interruptor technique. (This will be discussed in more detail in the next section.) Once the ohmic drop was measured, the overpotential could be calculated.

(ii) Resistance Measurement----Interruptor Technique

For the purpose of engineering analysis, it was of interest to learn how the resistance of

the electrolyte could be affected by bubble formation. In addition, in order to derive the overpotential of the cathode from the overpotential measurement mentioned in the last section, we needed to determine the magnitude of the resistances of the electrolyte. For these purposes, a classical method----the interruptor technique---- was used to determine the ohmic drop experimentally.

(a) Basic Theory

Usually, when a voltage measurement is made between a reference electrode and a working electrode, V_m , it includes the sum of three terms: the overpotential of the working electrode, η , the equilibrium potential difference between the working electrode and the reference electrode, ΔE , and the ohmic drop from the capillary tip of the reference electrode to the surface of the working electrode, IR ;

$$\text{i.e. } V_m = \eta + \Delta E + IR \quad \text{_____} \quad (2)$$

If the current, I , is interrupted suddenly, i.e. $I \rightarrow 0$, the ohmic drop vanishes for all practical purposes instantaneously. Therefore, if a fast responding voltage measuring instrument (usually a high quality oscilloscope) is connected to the reference electrode and the working electrode, an instantaneous drop in voltage will be observed. This voltage drop, ΔV , should correspond to the ohmic drop component between the capillary tip and the working electrode surface, IR . If ΔE is a known factor then the overpotential, η , can be calculated.

The principle of this technique is simple. However, in order for this principle to work, we have to assume that the decay of the voltage drop caused by the ohmic resistance is rapid in comparison to the decay of overpotentials of various sorts (i.e. charge transfer, mass transfer, & etc.). Usually, the decay of the concentration overpotential is relatively the slowest. The rate of the decay of charge transfer overpotential varies greatly depending on the nature of the electrode reaction. Let us estimate the order of magnitude of the time of decay in our system: J. Newman¹⁸ has shown that the decay time is inversely proportional to the exchange current density. He calculates the time constant of the decay of charge to be 0.51 msec for an exchange

current of 1 mA/cm^2 and a double layer capacity of $20 \mu\text{F/cm}^2$ at 25°C . For the polished electrode used in this study, the exchange current density is estimated to be 0.0025 mA/cm^2 ; and the corresponding time constant for the decay of charge would be around 200 msec. The interruptor technique could resolve events in the microsecond range. Thus, the decay of charge was much slower than the decay of the voltage caused by the ohmic potential drop.

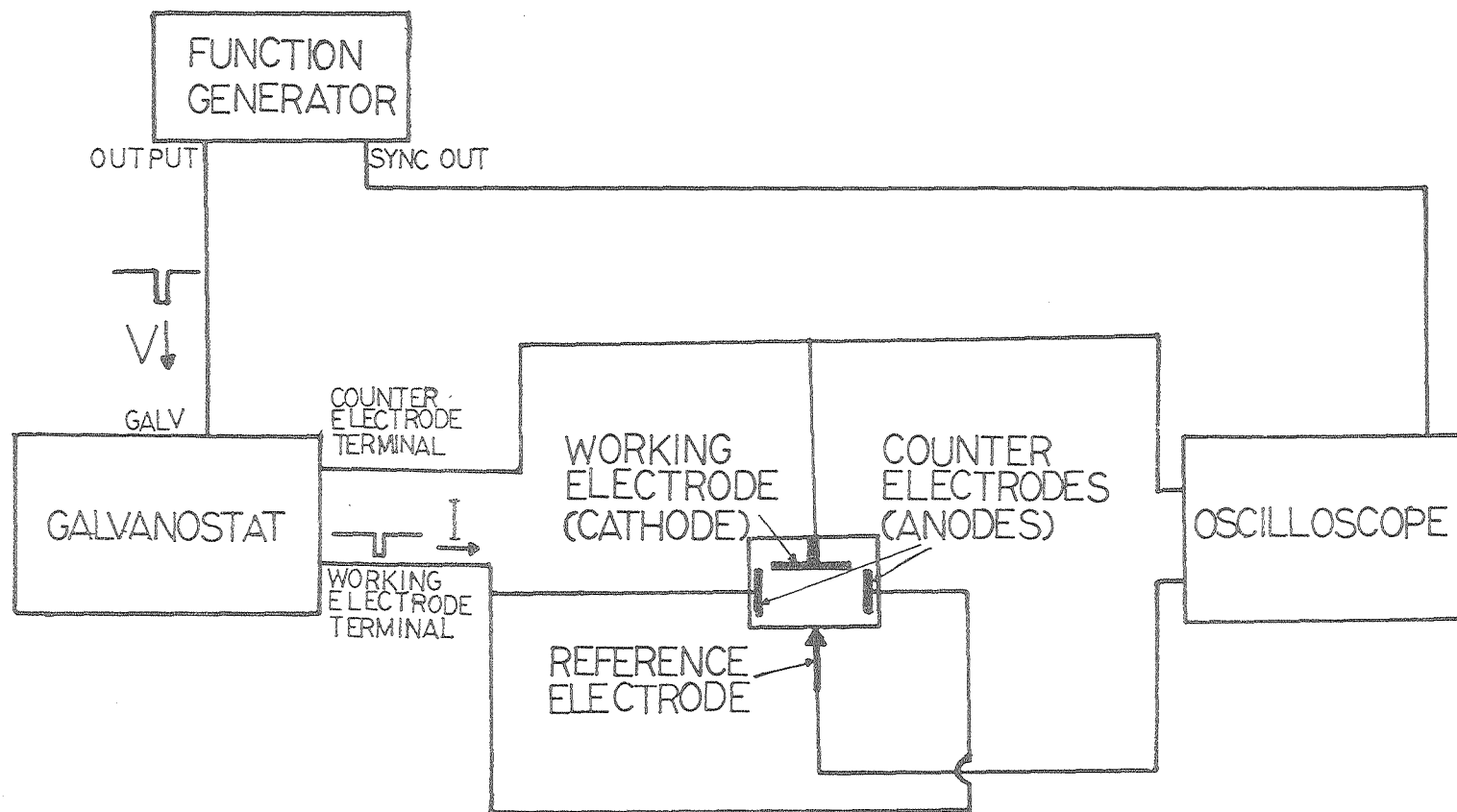
(b) Electrical Circuit

The electrical circuit is shown schematically in Figure (10). Basically, a galvanostat was used to supply a constant current for the electrolytic cell. A function generator was employed to generate voltage pulses, which in turn would drive the galvanostat to give current pulses. The voltage difference between the working electrode and the reference electrode was measured by an oscilloscope.

The galvanostat used was the Amel Model 551 Potentiostat-Galvanostat. This instrument had a special "mercury-wetted-relay" to switch on and off the current. This relay would be closed to allow current flow only at a voltage from $+3 \text{ V}$ up to $+5 \text{ V}$ or when the input was open. This device would prevent any back flow of current when the driving voltage was turned off; and therefore it would allow the galvanostat to operate with null steady-state current. This prevention of back flow of current is very important in determining the accuracy of the interruptor technique.

The function generator employed was an Interstate Electronics Corporation Model F77 Function Generator. This instrument could generate wave functions in various waveforms, amplitudes and widths. Usually, a 10 Hz square wave with unipolar signal of $+5 \text{ V}$ was used. The wave width was set asymmetrically in such a way that the ratio of the 5 V period to the 0 V period was 9:1. That means in every cycle the voltage output stayed at 5 V for about 0.09 sec. and then dropped down to 0 V for 0.01 sec. Therefore, in performing the interruptor technique, the cathode was forming bubbles at the pre-set current density in most of the time to keep the bubble environment unchanged.

For more accurate results, a Nicolet 1090A EXPLORER Digital Oscilloscope was used



XBL 805-9695

FIGURE (10) THE SCHEME OF THE ELECTRICAL CIRCUIT FOR INTERRUPTOR TECHNIQUE.

for the voltage measurement. It utilized an analog-to-digital converter (ADC) to measure the input signals at intervals of 500 nanoseconds or longer. The ADC could measure the signal with a resolution of one part in 4,000, and store the results in a digital memory.

(c) Estimation of the Incremental Resistance caused by Bubbles, ΔR_b

Since gas bubbles are non-conductive, it is expected that electrolyte containing bubbles will have higher resistance than that without bubbles. For the purpose of engineering analysis, it is interesting to find out how the resistance can be raised by the presence of bubbles.

The incremental resistance caused by bubbles, ΔR_b , is defined as the difference between the resistance of the electrolyte containing gas bubbles, R_g , and the resistance of the electrolyte without bubbles, R_{ng} :

$$\Delta R_b = R_g - R_{ng} \quad (3)$$

In the interruptor technique, the measured ohmic drop was actually equal to $I(R_g)$, and this can be expressed in terms of both $I(R_{ng})$ and $I(\Delta R_b)$:

$$\text{i.e. } I(R_g) = I(R_{ng}) + I(\Delta R_b) \quad (4)$$

In order to find ΔR_b , we have to estimate $I(R_{ng})$. Since the geometric arrangement of the electrodes was quite complicated, no simple calculation could be used to estimate $I(R_{ng})$. However, by experience, we found that it was possible to make an engineering estimation of $I(R_{ng})$ by using the following two facts:

- (1) By experience, it was found that ΔR_b was negligible at low current densities (e.g. $< 10 \text{ mA/cm}^2$), especially under high flow rate. This was because the bubbles were very tiny and well separated. In this case, $I(R_g)$ measured was very close to $I(R_{ng})$.
- (2) The current distribution of an electrochemical system is characterized by the Wagner Number, W :

$$W = Kb/LJ \text{ _____ (5)}$$

where K = the conductivity of the electrolyte, b = the Tafel slope for the overpotential curve, L = the characteristic length of the system, and J = current density. In the same system, L is fixed, therefore the current distribution is characterized only by Kb/J . Since K , b , and J are controllable factors, the current distribution can be kept similar by changing these factors accordingly.

The basic idea of this method was to make use of fact (1) to estimate the $I(R_{ng})$ at a high current density from the $I(R_g)$ measured at a low current density and a high flow rate. The first problem for this approach was that the current distributions were not the same at high and low current densities for the same electrolyte system. The second problem was that the ohmic drop, $I(R_g)$, was not measurable at very low current density with a highly conductive 5M KOH, because both R_g and I were too small. In order to solve these difficulties, we made use of fact (2). If a very dilute KOH solution (e.g. < 0.05M) was used to replace the 5M KOH, the R_{ng} would be high enough to make $I(R_{ng})$ measurable. Also, since the conductivity had been decreased, the current distribution at a low current density should correspond to that at a high current density in the 5M KOH solution. Therefore, by manipulating K and J around, the $I(R_{ng})$'s at high current densities in 5M KOH could be estimated from the $I(R_g)$'s measured at low current densities and high flow rates in dilute solutions. Then ΔR_b could be calculated by subtracting the R_{ng} from the R_g measured by the interruptor technique.

(III) OBSERVATIONS FROM MOTION PICTURES

The electrodes, according to their gas evolution behaviors, may be classified into: (1) a "normally behaving" group, and (2) a "strangely behaving" group. The first refers to those electrodes that generate even-sized bubbles along the same level as generally expected. The polished and the sanded electrodes belong to this group. The "strangely behaving" group refers to those electrodes that generate bubbles at various rates depending on the local features. The bubble may be of different sizes by orders of magnitude. The resulting resistances behave quite strangely too. This group includes the pyramidal and the grooved electrodes. A summary of the differences in the gas evolution behaviors of these two groups of electrodes is given in Table (1).

(1) Group (1)-----Polished and Sanded Electrodes

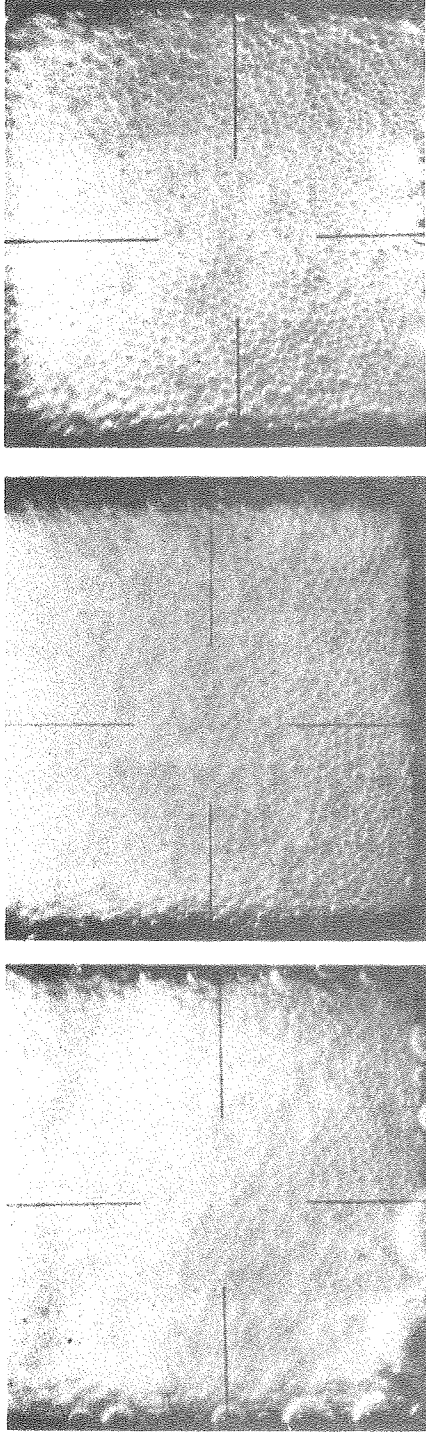
(i) Bubble Size and Nucleation Site Distribution

Generally, the group (1) electrodes behaved very similarly with respect to gas evolution. They differed mainly in the size of bubbles generated on them. Comparing the bubble sizes, the order is as follows: the polished electrode > the crosswise sanded electrode > the parallel sanded electrode. Figure (11) gives an example with the pictures of the gas bubbles generated at 1 A/cm^2 in stagnant solution for the group (1) electrodes. Usually, the newly generated bubbles were very small, but their sizes increased rapidly as they rose along the electrode. Most of the bubble sizes were of the same order of magnitude. However, bubbles were sometimes larger along the epoxy-nickel interstices before they left the electrode. This case was particularly true for the polished electrode.

The bubble size and the density of active nucleation sites increased as the current density was increased. To illustrate this phenomenon, Figures (12), (13) and (14) show the pictures of the bubble formations at various current densities for each of the group (1) electrodes respec-

TABLE (1) SUMMARY OF THE DIFFERENCES IN THE GAS EVOLUTION BEHAVIORS OF THE TWO GROUPS OF ELECTRODES

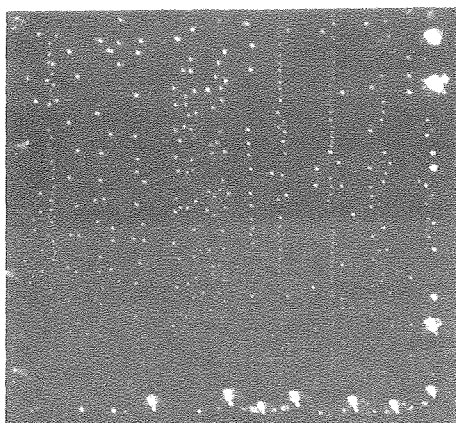
	<u>NORMALLY BEHAVING GROUP :</u> POLISHED & SANDED ELECTRODES	<u>STRANGELY BEHAVING GROUP :</u> GROOVED & PYRAMIDAL ELECTRODES
BUBBLE SIZE	MOST BUBBLES ARE OF THE SAME ORDER OF MAGNITUDE.	MIXTURE OF VERY TINY AND LARGE BUBBLES.
NUCLEATION SITE DISTRIBUTION	NUCLEATION SITES ARE UNIFORMLY DISTRIBUTED.	DIFFERENT LOCAL FEATURES HAVE DIFFERENT ACTIVITY IN GENERATING BUBBLES.
EFFECT OF INCREASING CURRENT DENSITY	MORE NUCLEATION SITES ARE ACTI- VATED, AND THE BUBBLE SIZE BECOMES LARGER.	MORE NUCLEATION SITES FOR TINY AND EMULSIFIED BUBBLES ARE ACTIVATED ON THE GROOVE FACES. THE LARGE BUBBLES IN GROOVES INCREASE IN SIZE. THE EFFECT ON THE CROSSWISE GROOVED ELECTRODE IS MORE COMPLICATED.
EFFECT OF FORCED FLOW	THE SIZE AND THE DENSITY OF THE BUBBLES ARE REDUCED BY INCREAS- ING FLOW RATE.	MAIN EFFECT IS TO REMOVE THE TINY AND THE EMULSIFIED BUBBLES FROM THE SURFACE OF THE ELECTRODE. THE EFFECT ON THE BUBBLES IN GROOVES VARIES WITH ELECTRODES.



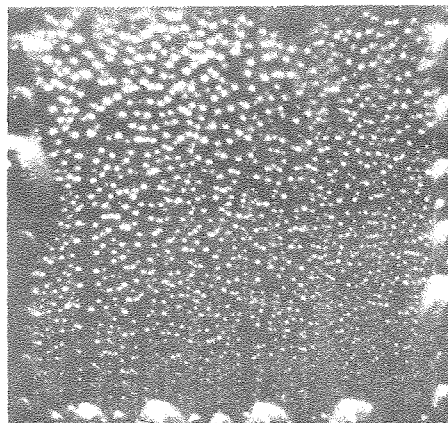
(A) POLISHED ELECTRODE,  (B) PARALLEL SANDED ELECTRODE,  (C) CROSSWISE SANDED ELECTRODE, 

XBB-800-12058

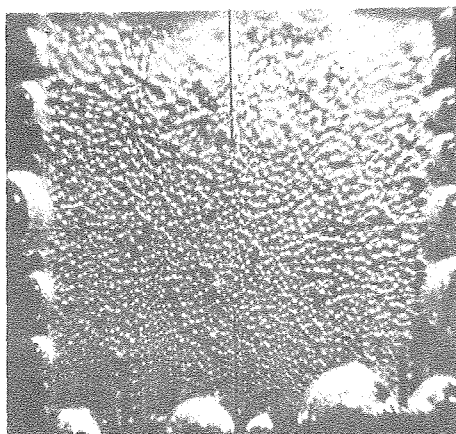
FIGURE (11) BUBBLE FORMATIONS ON THE GROUP (1) ELECTRODES AT 1 A/cm² IN STAGNANT ELECTROLYTE.



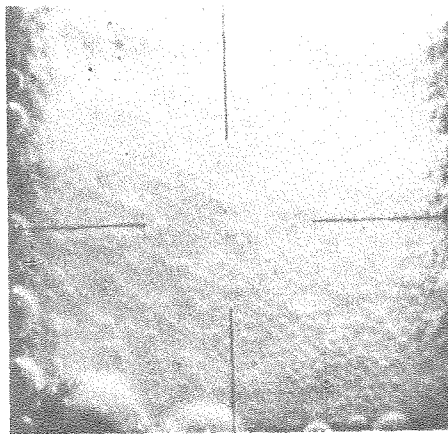
(A) $J = 1 \text{ mA/cm}^2$



(B) $J = 10 \text{ mA/cm}^2$



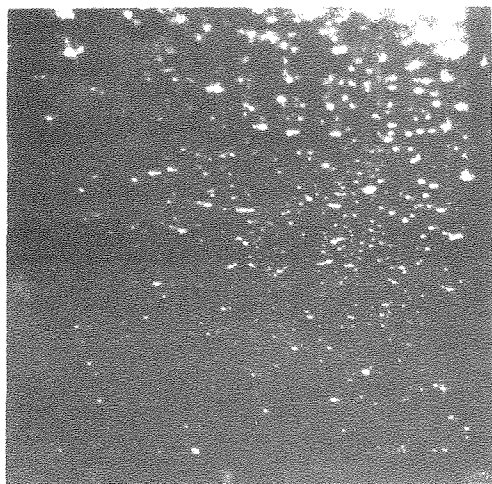
(C) $J = 100 \text{ mA/cm}^2$



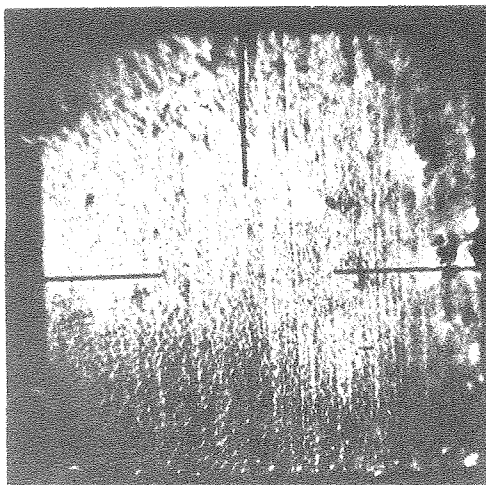
(D) $J = 1000 \text{ mA/cm}^2$

FIGURE (12) BUBBLE FORMATIONS ON THE POLISHED ELECTRODE AT VARIOUS CURRENT DENSITIES IN STAGNANT SOLUTION.

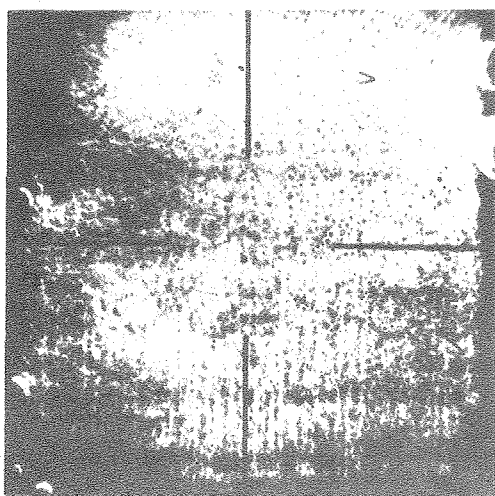
XBB-800-12059



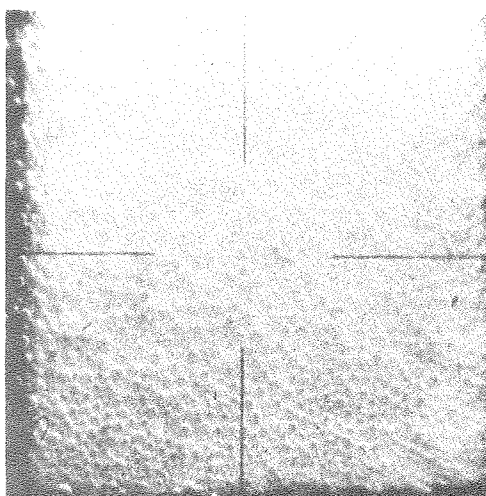
(A) $J = 1 \text{ mA/cm}^2$



(B) $J = 10 \text{ mA/cm}^2$

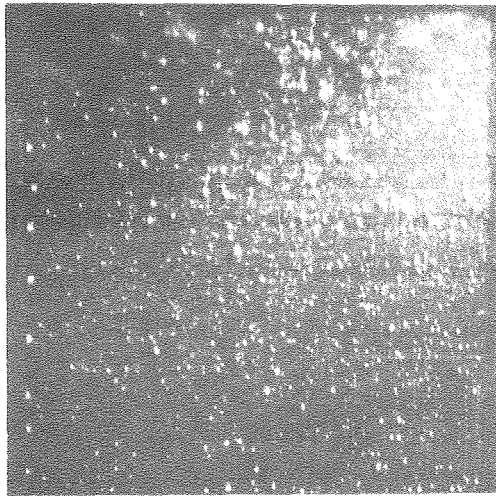


(C) $J = 100 \text{ mA/cm}^2$

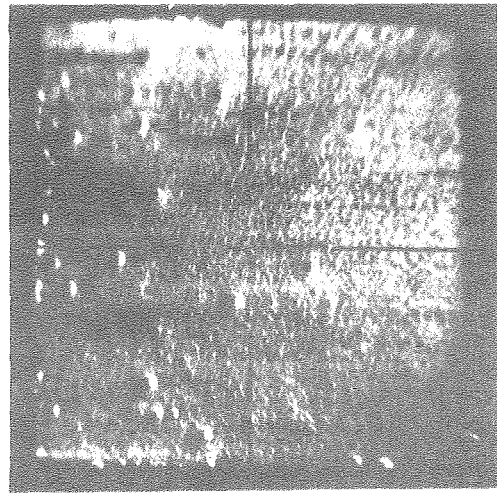


(D) $J = 1000 \text{ mA/cm}^2$

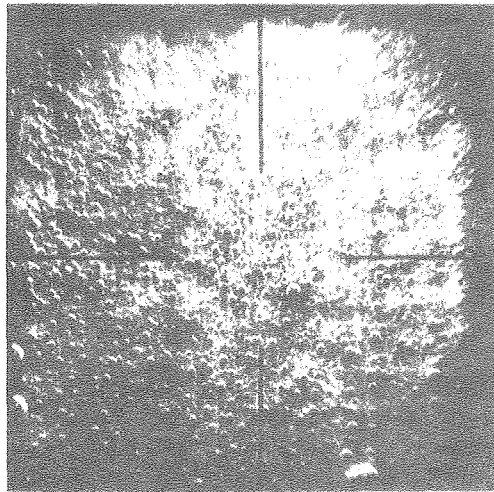
FIGURE (13) BUBBLE FORMATIONS ON THE PARALLEL SANDDED ELECTRODE AT VARIOUS CURRENT DENSITIES IN STAGNANT SOLUTION.



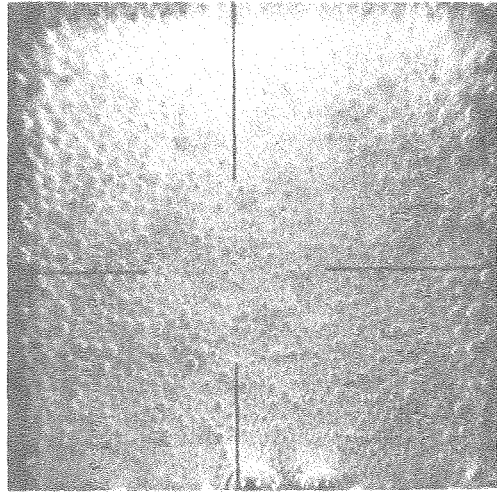
(A) $J = 1 \text{ mA/cm}^2$



(B) $J = 10 \text{ mA/cm}^2$



(C) $J = 100 \text{ mA/cm}^2$



(D) $J = 1000 \text{ mA/cm}^2$

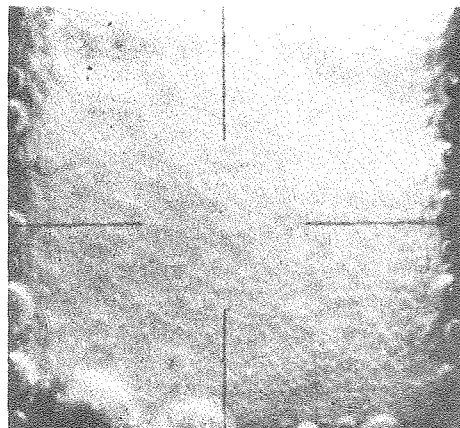
FIGURE (14) BUBBLE FORMATIONS ON THE CROSSWISE SANDED ELECTRODE AT VARIOUS CURRENT DENSITIES IN STAGNANT SOLUTION.

tively. At very low current densities (e.g. $\sim 1 \text{ mA/cm}^2$), the bubbles were very small ($\leq 50 \mu\text{m}$) and well scattered. For the sanded electrodes, the bubbles were quite evenly distributed over the whole surface. However, the polished electrode had more active nucleation sites along the edges than on the surface. Usually, the bubbles at these edge sites could grow much larger before they took off. (In the photographs, a lot of the bubbles appearing on the electrode surfaces were not generated there. They actually came from the nucleation sites along the lower edges and in the lower portions of the electrodes.)

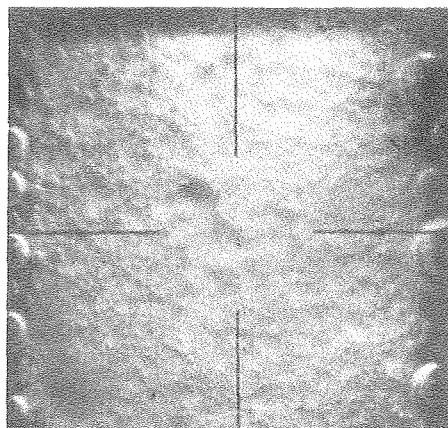
As the current density was increased, more and more nucleation sites were activated to generate bubbles. This caused all three electrodes to have uniform distributions of active nucleation sites. At the same time, the bubbles became larger and rose faster. Coalescence began to take place. At current density higher than 40 mA/cm^2 , the bubbles became closely packed. This was the point where the incremental ohmic drop caused by the bubbles became significant. After this point, the effect of current change was mainly on the bubble size----it increased with increasing current density.

(ii) Effects of Forced Flow

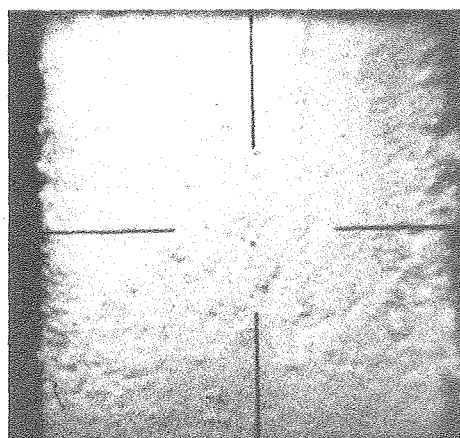
Optical study of the effect of forced flow was done only in the high current density region ($> 40 \text{ mA/cm}^2$). The effects of the flow were similar for all of the group (1) electrodes. Figure (15), (16) and (17) show the bubble formations of the group (1) electrodes at 1 A/cm^2 under various flow rates. Basically, the forced flow would remove the gas bubbles faster. This causes the bubbles to leave the nucleation sites at earlier stages, and decreases the residence time of the bubbles at the electrode. Therefore, the bubble size, especially at the edge, decreased as the flow rate was increased. The forced flow not only reduced the bubble size, it also decreased the coverage of bubbles on the electrode. At low flow rates ($U_0 < 40 \text{ cm/sec}$, i.e. in laminar region), most of the bubbles were still closely packed, and were covering the whole electrode. At 40 cm/sec (around the transition region), the gas bubble layer became less closely packed. Because of the reduction in the density of bubble coverage layer, some of the dense tiny bubbles initiating underneath were revealed. These tiny bubbles were usually taken in by the large bubble before they had the chance to grow bigger. At higher flow rates (e.g. $U_0 = 83 \text{ cm/sec}$ or 135 cm/sec), the turbulence removed the bubbles unevenly from the



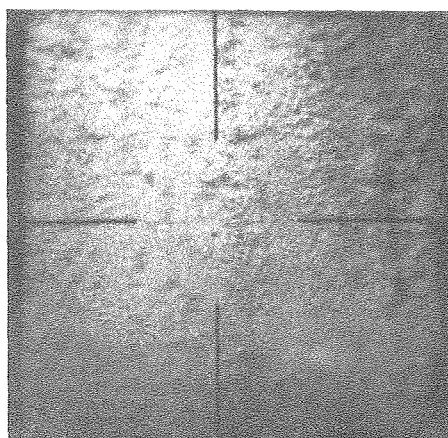
(A) IN STAGNANT SOLUTION



(B) $U_0 = 40$ CM/SEC
 $Re = 1960$

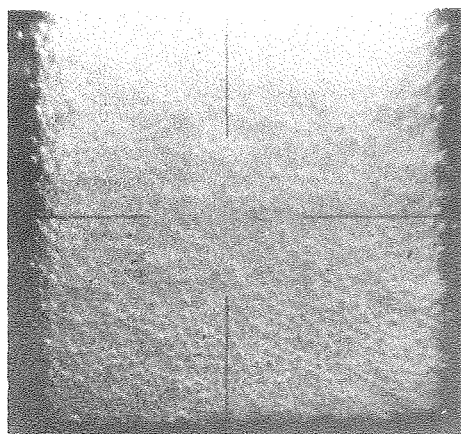


(C) $U_0 = 83$ CM/SEC
 $Re = 4250$

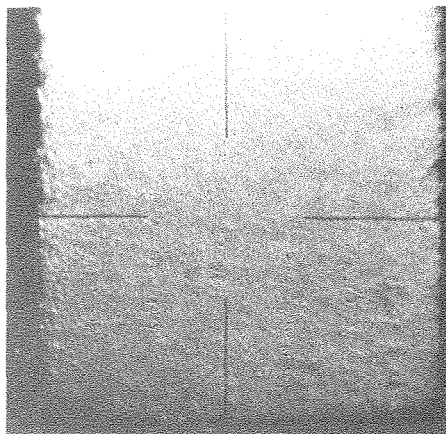
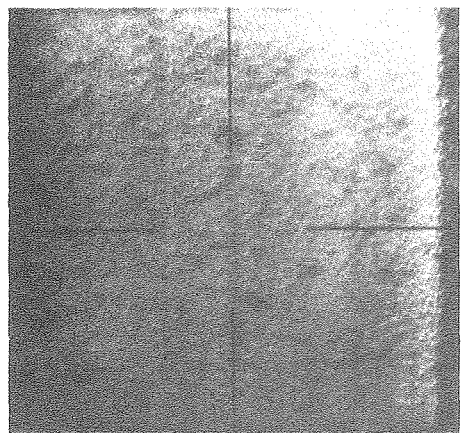
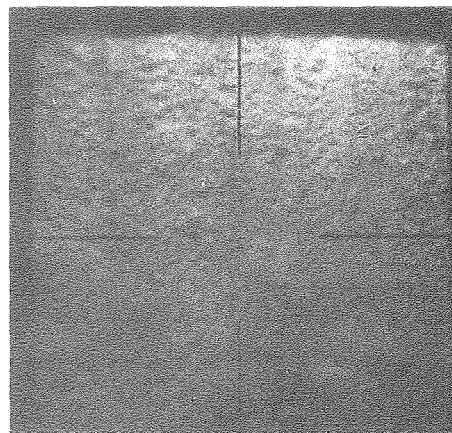


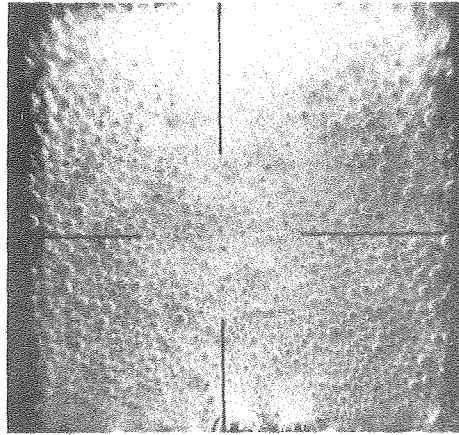
(D) $U_0 = 135$ CM/SEC
 $Re = 6600$

FIGURE (15) BUBBLE FORMATIONS ON THE POLISHED ELECTRODE AT 1 A/cm^2 UNDER VARIOUS FLOW RATES.



(A) IN STAGNANT SOLUTION

(B) $U_0 = 40$ CM/SEC
 $Re = 1960$ (C) $U_0 = 83$ CM/SEC
 $Re = 4250$ (D) $U_0 = 135$ CM/SEC
 $Re = 6600$ FIGURE (16) BUBBLE FORMATIONS ON THE PARALLEL
SANDED ELECTRODE AT 1 A/cm^2 UNDER
VARIOUS FLOW RATES.



(A) IN STAGNANT SOLUTION

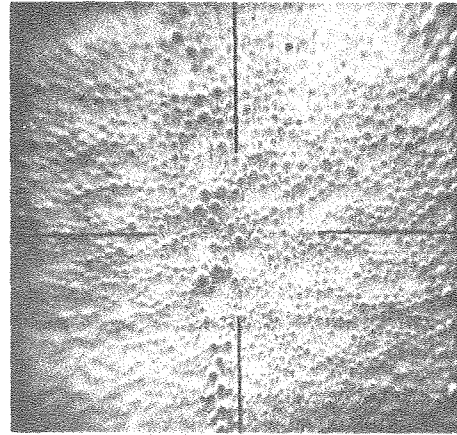
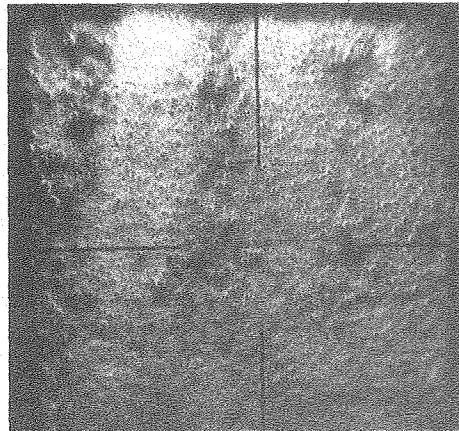
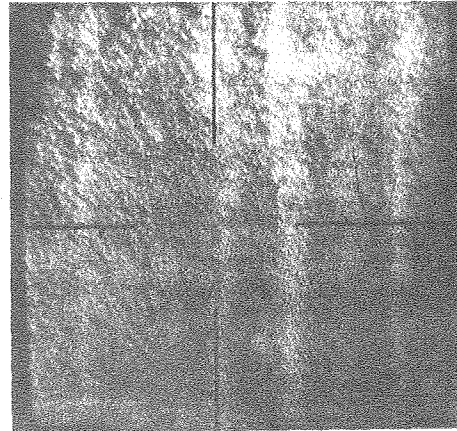
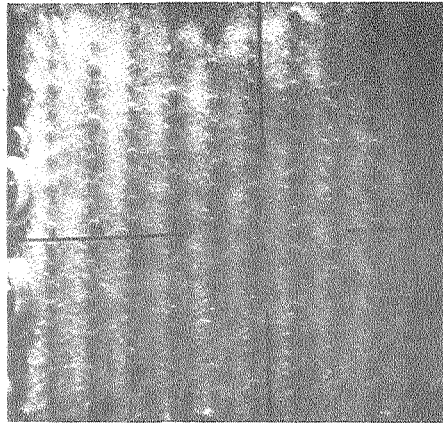
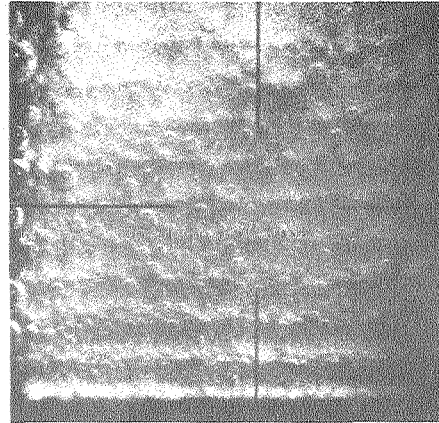
(B) $U_0 = 40$ CM/SEC
 $Re = 1960$ (C) $U_0 = 83$ CM/SEC
 $Re = 4250$ (D) $U_0 = 135$ CM/SEC
 $Re = 6600$

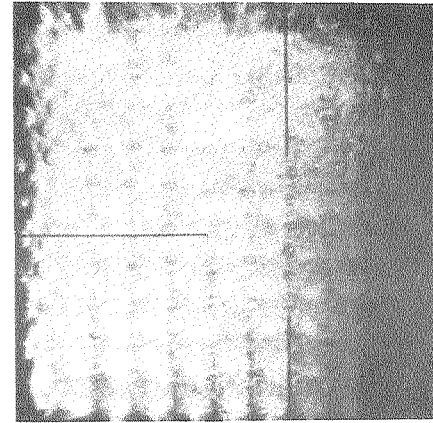
FIGURE (17) BUBBLE FORMATIONS ON THE CROSSWISE SANDED ELECTRODE AT 1 A/cm^2 UNDER VARIOUS FLOWS.



(A) PARALLEL GROOVED
ELECTRODE, 



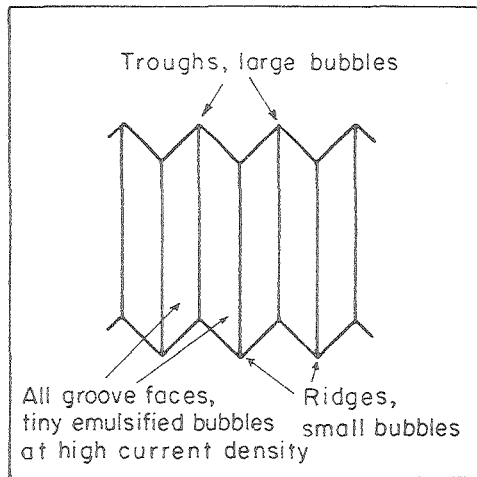
(B) CROSSWISE GROOVED
ELECTRODE, 



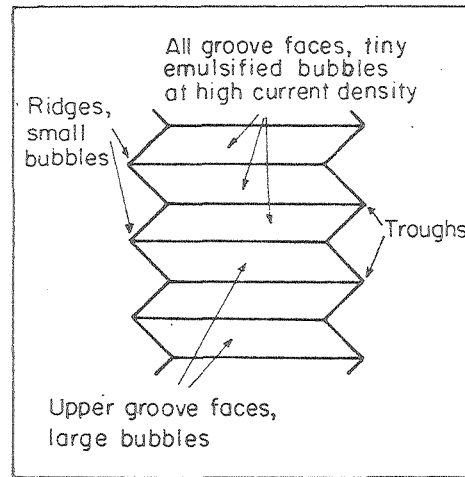
(C) PYRAMIDAL ELECTRODE,


XBB-800-12061

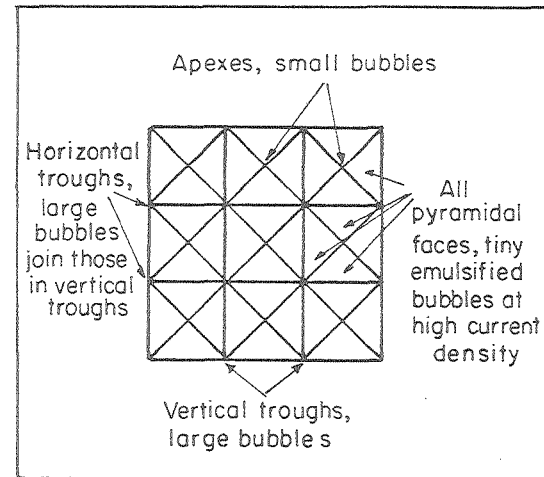
FIGURE (19) BUBBLE FORMATIONS ON THE GROUP (2) ELECTRODES AT 1 A/cm^2
IN STAGNANT ELECTROLYTE.



(A) Parallel Grooved Electrode



(B) Crosswise Grooved Electrode



(C) Pyramidal Electrode

XBL 808-5629

FIGURE (20) THE DISTRIBUTION OF THE ACTIVE NUCLEATION SITES ON GROUP (2) ELECTRODES.

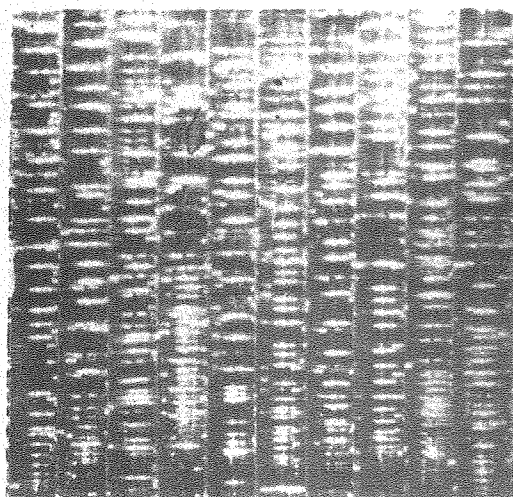
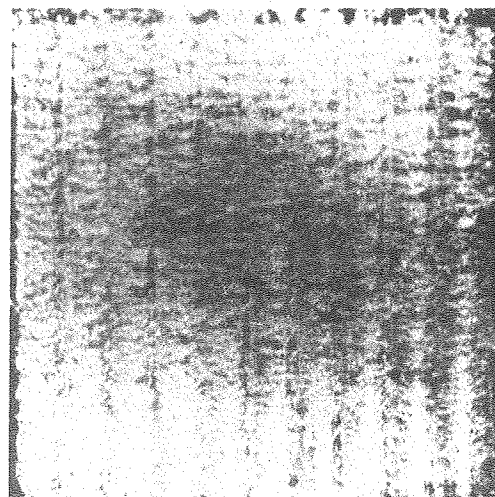
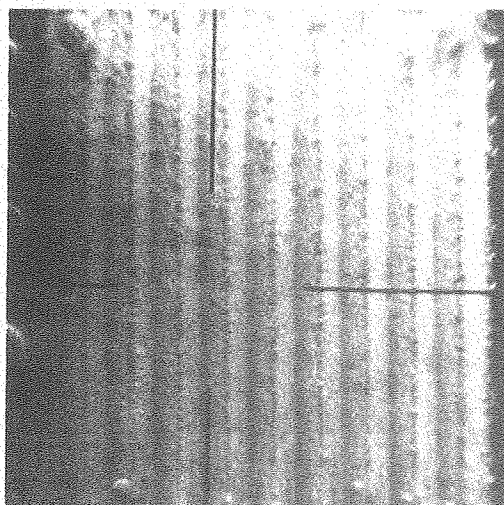
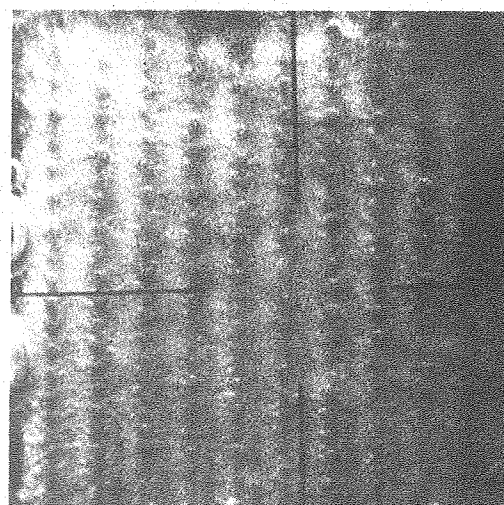
(A) $J = 1 \text{ mA/cm}^2$ (B) $J = 10 \text{ mA/cm}^2$ (C) $J = 100 \text{ mA/cm}^2$ (D) $J = 1000 \text{ mA/cm}^2$

FIGURE (21) BUBBLE FORMATIONS ON THE PARALLEL GROOVED ELECTRODE AT VARIOUS CURRENT DENSITIES IN STAGNANT SOLUTION.

As the current density was increased ($> 4 \text{ mA/cm}^2$), some points on the groove faces were activated to generate bubbles. These nucleation sites increased with the current density. All the bubbles floated up along the grooves without coalescence. As a result, there were a few streams of bubbles in each groove. (See Figure (21)(B).)

At current density around 40 mA/cm^2 , the bubbles became closely packed; and some very tiny, emulsified bubbles ($< 10 \mu\text{m}$) were generated all over the groove faces. These tiny and emulsified bubbles filled up all the grooves and covered the whole electrode. It was hard to tell the actual size of the larger bubbles in the troughs. One simple trick to solve this problem was to pass a very low flow rate to remove just the surface emulsified bubbles. It was found that the bubbles in each trough had coalesced and formed a single bubble stream. As the current density was increased, the trough bubbles became larger ($> 100 \mu\text{m}$), and the emulsified bubbles became thicker and denser. (See Figure (21)(C) and (D).)

(b) Crosswise Grooved Electrode

Figure (22) shows how the bubble distribution looks at various current densities in stagnant solution. At very low current densities ($< 2 \text{ mA/cm}^2$), most of the bubble growth occurred on the upper groove faces. They stayed there and grew into large bubbles ($> 300 \mu\text{m}$) before they left the grooves (Figure (22)(A)). At the same time, some smaller bubbles ($\sim 30\text{-}45 \mu\text{m}$) were formed on the ridges. As the current density was increased, the rate of evolution of both large and small bubbles increased. Since the number of large bubbles that could stay in the grooves was limited by the space available, the number of these bubbles on the electrode did not increase as much as the small bubbles. These large bubbles had shorter residence time in the grooves, and the frequency of their evolution was higher.

At current densities higher than 4 mA/cm^2 , the ridges and the groove faces started to generate a lot of tiny and emulsified bubbles ($< 10 \mu\text{m}$). (See Figure (22)(B).) As the current density was increased to around 40 mA/cm^2 , these emulsified bubbles filled up all the space in the grooves. (See Figure (22)(C).) Up to current density of 200 mA/cm^2 , the stirring effect caused by the bubbles was so vigorous that no bubble could stay on the upper portion of the electrode to grow larger. More large bubbles were "kicked out" of the grooves. These

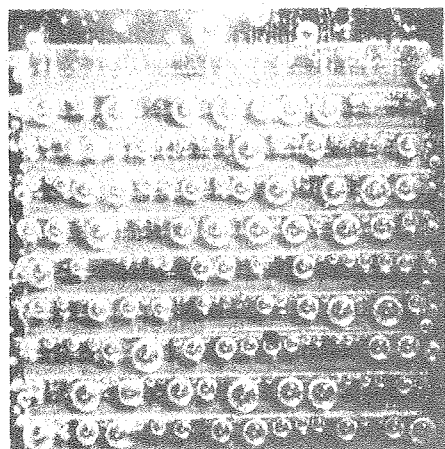
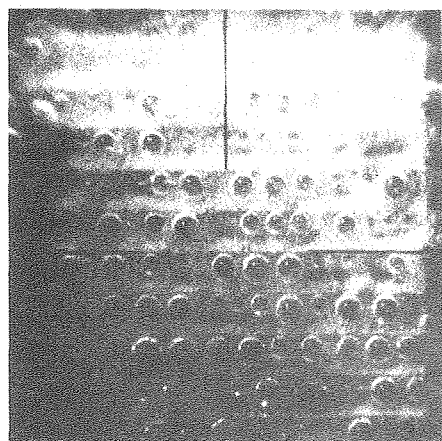
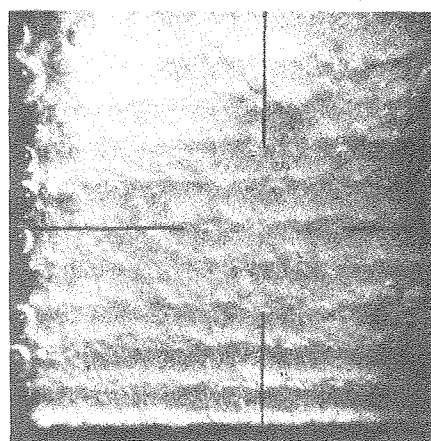
(A) $J=1 \text{ mA/cm}^2$ (B) $J=10 \text{ mA/cm}^2$ (C) $J=100 \text{ mA/cm}^2$ (D) $J=1000 \text{ mA/cm}^2$

FIGURE (22) BUBBLE FORMATIONS ON THE CROSSWISE GROOVED ELECTRODE AT VARIOUS CURRENT DENSITIES IN STAGNANT SOLUTION.

XBB-800-12066

bubbles were only about 135 to 225 μm (vs $\sim 300 \mu\text{m}$ as at lower current densities). At current density of 1 A/cm^2 , this "kicking out" of bubbles was very vigorous and no large bubbles were able to stay in the grooves at all. The electrode was then covered completely with a layer of large bubbles of 135 to 225 μm (Figure (22)(D)).

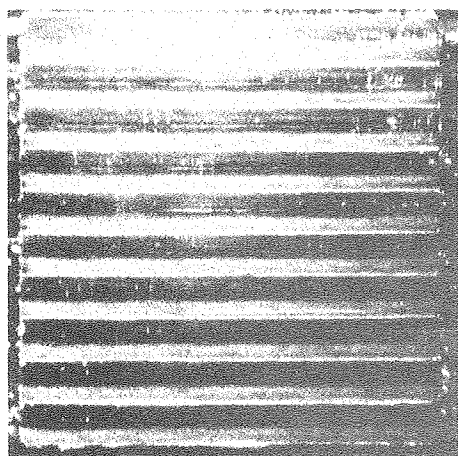
For this special electrode, there was an interesting shift of nucleation sites. Initially, when the reaction started, the bubbles were generated in the troughs rather than on the upper faces of the grooves (Figure (23)(A)). However, before they could grow larger, they floated up to the upper faces of the grooves and stuck there (Figure (23)(B)). Then they grew into larger bubbles (Figure (23)(C) and (D)). After these bubbles left the grooves, new bubbles were initiated on the upper faces rather than on the troughs (Figure (23)(D)). This may be due to the fact that the residual gas left behind by the large bubbles provides more active nucleation sites than the troughs.

(c) Pyramidal Electrode

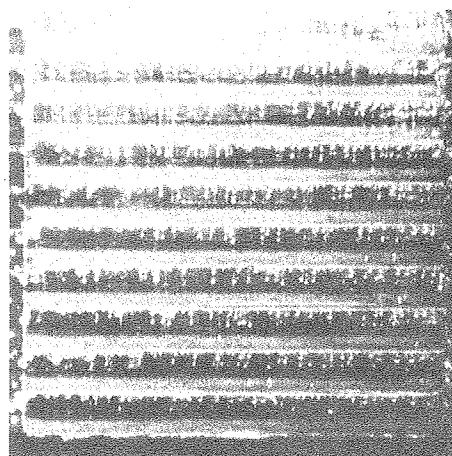
It was much harder to make photographic observations with the pyramidal electrode than the others, especially at low current densities. This was due to the light reflection problem caused by the faces of the pyramids. With the movies, it was barely possible to see the events of gas bubble evolution by tracing the moving spots. However, there was no easy way to illustrate these events clearly by just a few static pictures.

At low current densities ($\leq 1 \text{ mA}/\text{cm}^2$), bubbles ($\sim 50 \mu\text{m}$) were generated along the base lines of the pyramids (Figure (24)(A)). Those bubbles nucleated from the horizontal base lines were drawn to the bubble streams in the vertical grooves right after they were generated. All these bubbles floated up along the vertical grooves without coalescence. There were also a few small bubbles evolving at the apexes. They were about 30-45 μm in diameter.

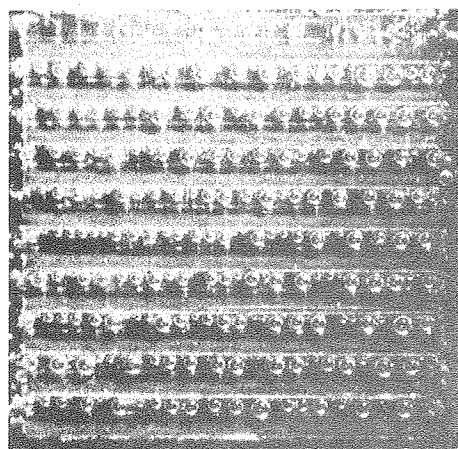
As the current density was increased, both the quantity and the size of the bubbles in the grooves increased (e.g. $\sim 100 \mu\text{m}$ at 2 mA/cm^2). At around 10 mA/cm^2 , emulsified bubbles ($< 10 \mu\text{m}$) started to form on the faces of the pyramids too. (See Figure (24)(B).) As the current density became higher than 40 mA/cm^2 , the whole electrode was filled with these



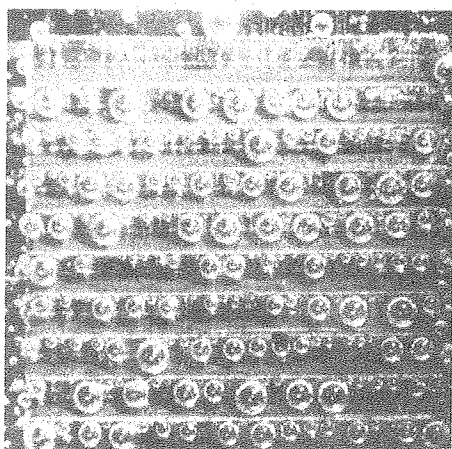
(A) AT THE BEGINNING



(B) AFTER 10 SECONDS



(C) AFTER 31 SECONDS



(D) AFTER 10 MINUTES

FIGURE (23) THE SHIFTING OF NUCLEATION SITES ON THE CROSSWISE GROOVED ELECTRODE AT 1 mA/cm^2 IN STAGNANT SOLUTION.

XBB-800-12067

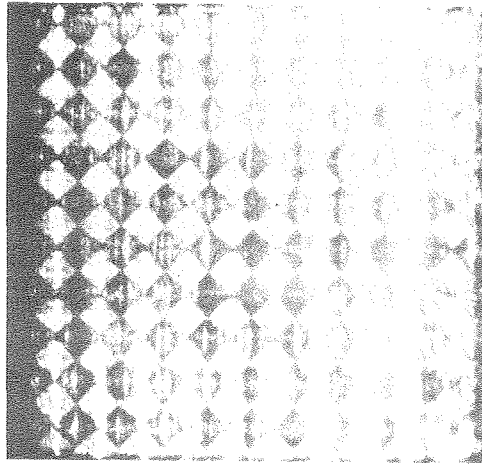
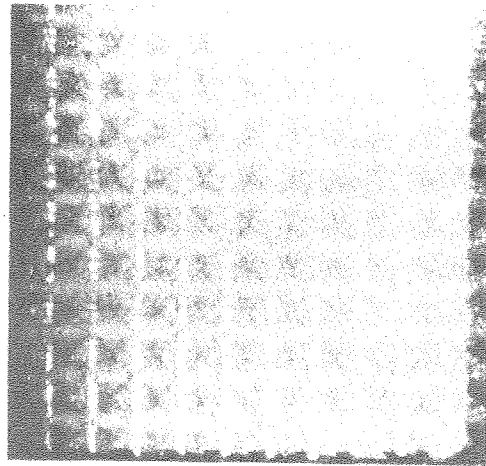
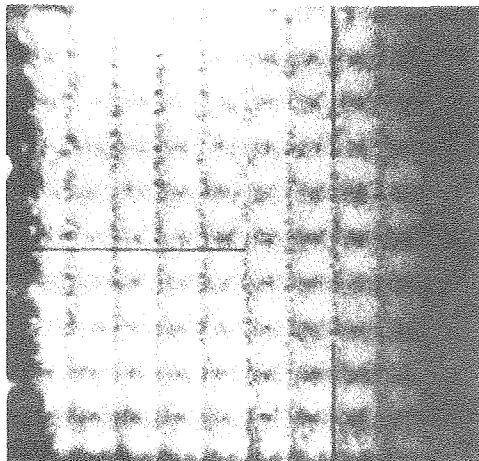
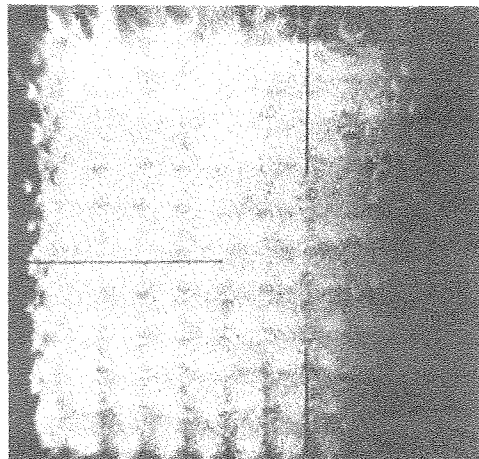
(A) $J=1\text{mA}/\text{cm}^2$ (B) $J=10\text{mA}/\text{cm}^2$ (C) $J=100\text{mA}/\text{cm}^2$ (D) $J=1000\text{mA}/\text{cm}^2$

FIGURE (24) BUBBLE FORMATIONS ON THE PYRAMIDAL ELECTRODE AT VARIOUS CURRENT DENSITIES IN STAGNANT SOLUTION.

XBB-800-12068

emulsified bubbles. The bubbles floating in the vertical troughs also became larger: they reached $\sim 135\text{-}180\ \mu\text{m}$ at $100\ \text{mA}/\text{cm}^2$ (Figure (24)(C)) and $\sim 230\text{-}300\ \mu\text{m}$ at $1\ \text{A}/\text{cm}^2$ (Figure (24)(D)).

(ii) Effects of Forced Flow

(a) Parallel Grooved Electrode

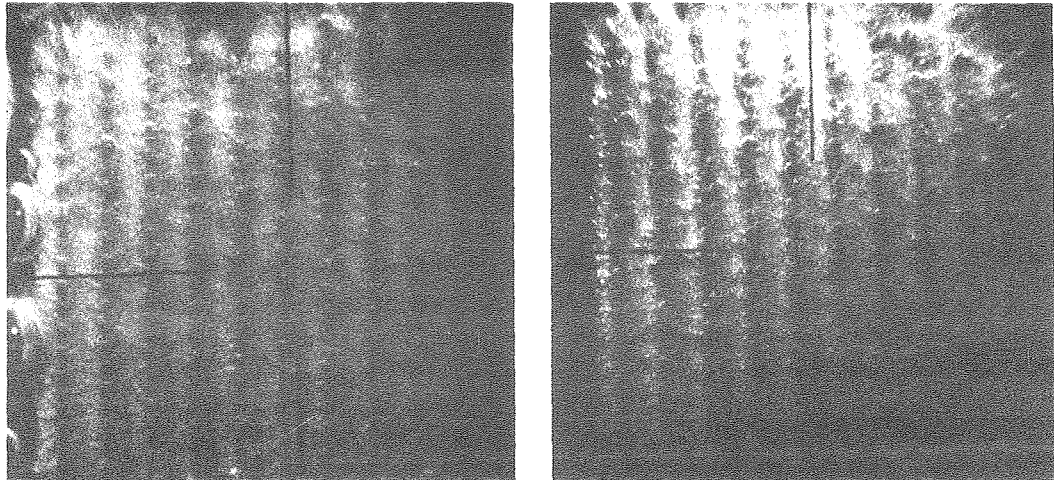
The main effect of the forced flow on this electrode was to remove the emulsified bubbles from the surface of the electrode. (See Figure (25).) The flow also entrained the trough bubbles more effectively.

(b) Crosswise Grooved Electrode

Since the bubble generation behavior of this electrode changed with current density, the effect of forced flow was different at various current densities.

At current densities lower than $200\ \text{mA}/\text{cm}^2$ (i.e. before the "kicking out" the large bubbles), the forced flow would remove the emulsified bubbles and the large bubbles in the grooves. See Figure (26) for an example at $100\ \text{mA}/\text{cm}^2$. At low flow rates (e.g. $40\ \text{cm}/\text{sec}$), fewer bubbles were allowed to stay in the grooves to grow larger. (Compare Figure (26)(A) and (B).) The bubbles usually left the grooves at smaller sizes ($\sim 315\ \mu\text{m}$, vs $\sim 360\ \mu\text{m}$ in stagnant solution). Great many of the emulsified bubbles were still trapped in the grooves. As the flow was increased (e.g. $87\ \text{cm}/\text{sec}$), it was possible to remove all the large bubbles, but not the emulsified bubbles. (See Figure (26)(C).)

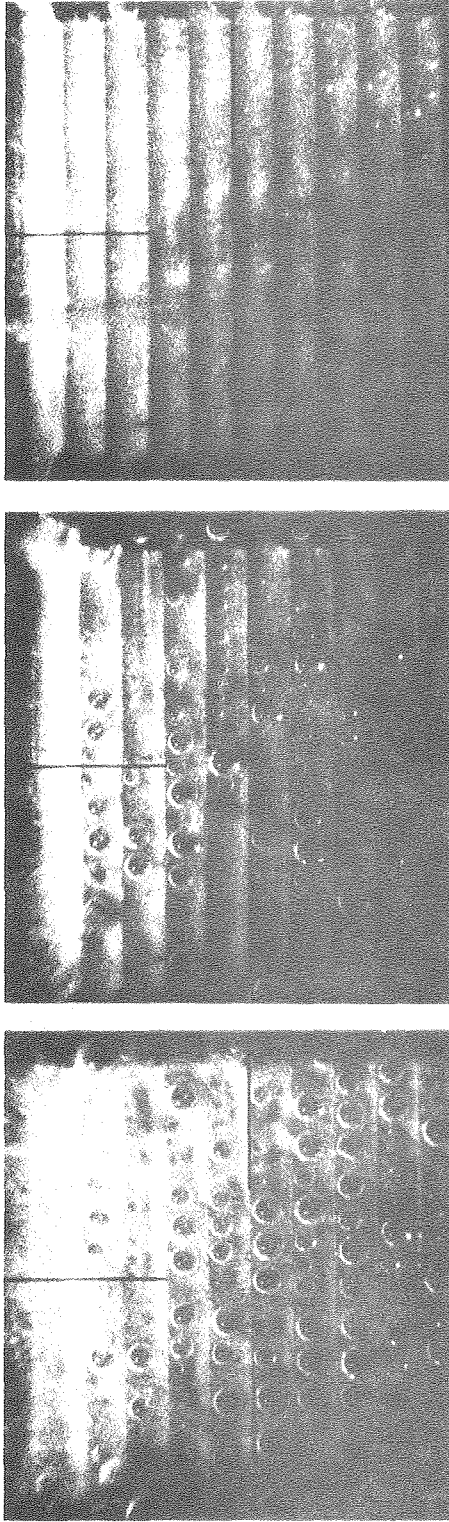
At higher current densities ($\geq 1000\ \text{mA}/\text{cm}^2$), no large bubbles could stay in the grooves, and the electrode was covered with a layer of gas bubbles of 135 to $225\ \mu\text{m}$. In this range, the main effect of the forced flow was to remove this surface bubble layer. (See Figure



(A) IN STAGNANT SOLUTION (B) $U_0=40$ CM/SEC, $Re=1960$

FIGURE (25) BUBBLE FORMATIONS ON THE PARALLEL GROOVED ELECTRODE AT 1 A/cm^2 (A) IN STAGNANT SOLUTION, AND (B) AT $U_0=40$ CM/SEC.

XBB-800-12069



(A) IN STAGNANT SOLUTION (B) $U_0=40$ cm/sec, $Re=1960$ (C) $U_0=87$ cm/sec, $Re=4250$

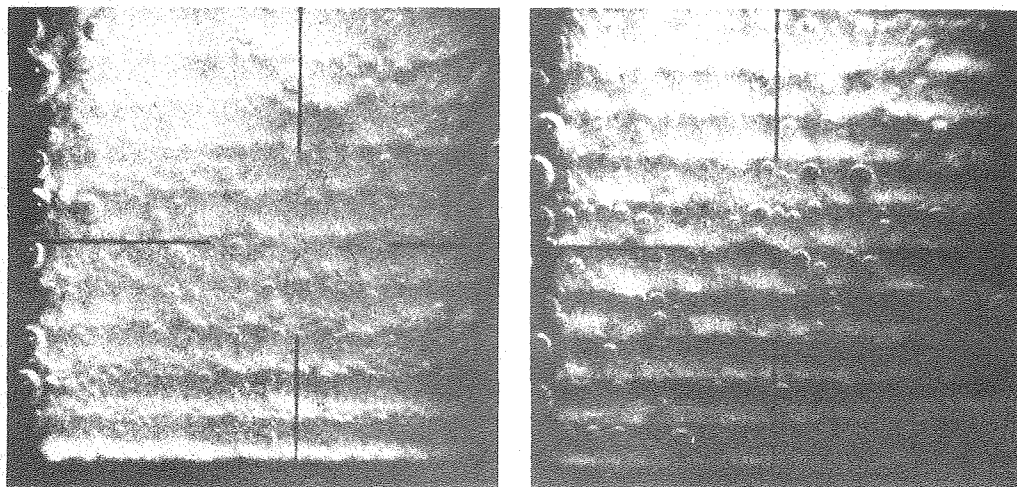
XBB-800-12072

FIGURE (26) BUBBLE FORMATIONS ON THE CROSSWISE GROOVED ELECTRODE AT 100 mA/cm^2 UNDER VARIOUS FLOW RATES.

(27).)

(c) Pyramidal Electrode

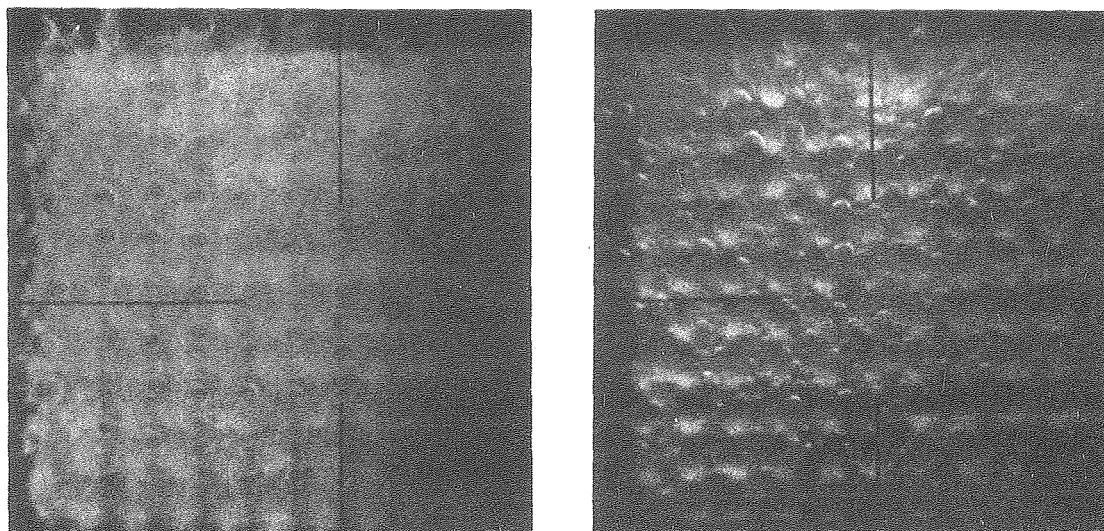
The effects of the forced flow on this electrode were very similar to those on the parallel grooved electrode. The forced flow helped to remove the emulsified bubbles from the surface, and caused the large trough bubbles to rise faster and be of smaller size. For example, at 100 mA/cm^2 , the trough bubbles had sizes ranging from 230 to $300 \mu\text{m}$ in stagnant solution; whereas those under forced flow of 40 cm/sec were around 130 to $220 \mu\text{m}$. (Compare Figure (28)(A) and (B).)



(A) IN STAGNANT SOLUTION (B) $U_0 = 40$ CM/SEC, $Re = 1960$

FIGURE (27) BUBBLE FORMATIONS ON THE CROSSWISE GROOVED ELECTRODE AT 1 A/cm^2 IN STAGNANT SOLUTION AND AT $U_0 = 40$ CM/SEC RESPECTIVELY.

XBB-800-12070



(A) IN STAGNANT SOLUTION. (B) $U_0=40$ cm/SEC, $Re=1960$.

FIGURE (28) BUBBLE FORMATIONS ON THE PYRAMIDAL ELECTRODE AT 1 A/cm² IN STAGNANT SOLUTION AND AT $U_0=40$ cm/SEC RESPECTIVELY.

XBB-800-12071

(IV) RESULTS OF ELECTRICAL MEASUREMENTS

(1) Overpotential Measurements

(i) In Stagnant Solution

The polarization curves of all the electrodes in stagnant solution are plotted in Figure (29). All of them obey the Tafel relation:

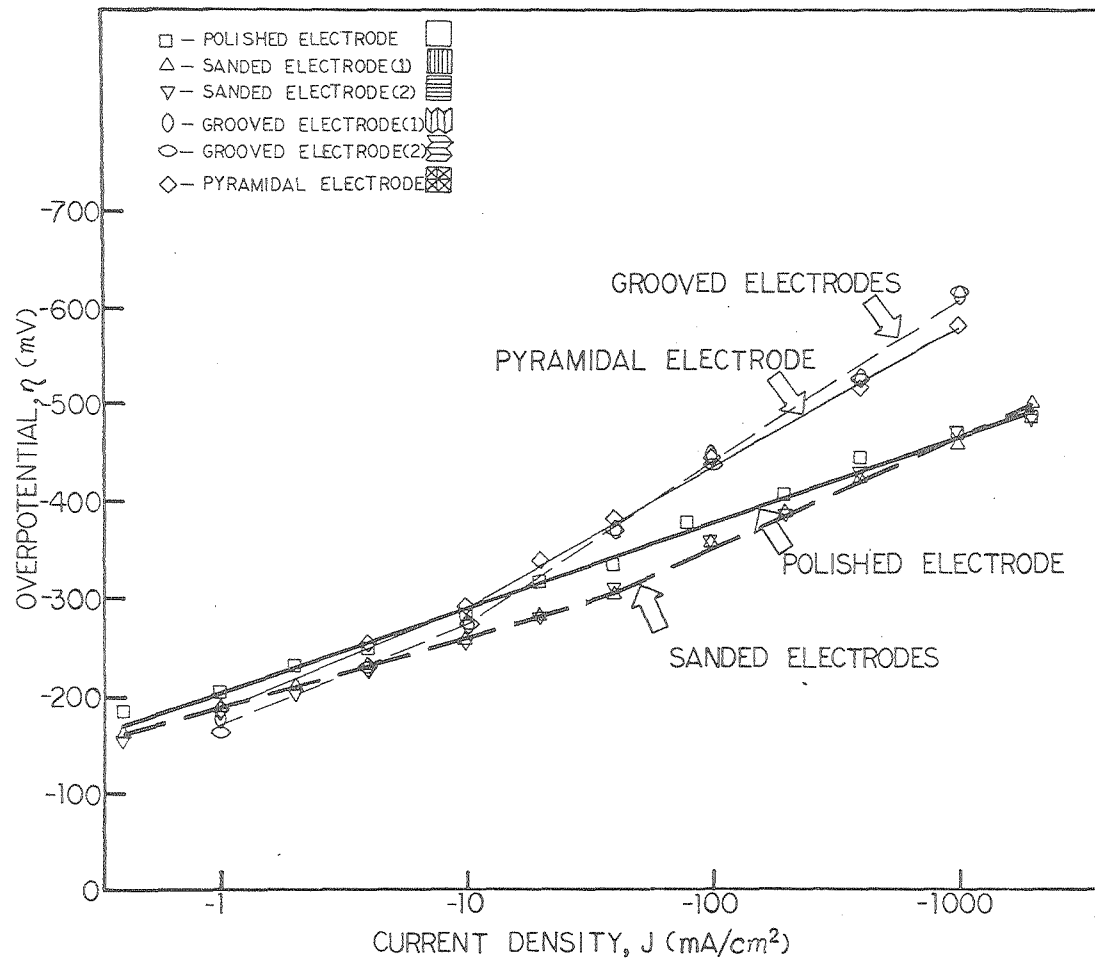
$$\eta = a - b \log(J) \quad (6)$$

where a and b are constants (b is called the Tafel slope, a constant). All the electrodes, except the polished one, have different Tafel slopes for the lower and the higher current density regions. The values of the slopes and the intercepts are listed in Table (2). The ranges of the literature values are also shown for comparison.

The orientation of the electrode seemed to have no effect on the polarization behavior. Both the grooved- and the sanded-electrodes had the same polarization curves in either parallel or perpendicular orientation to the flow.

The sanded electrodes were shown to have lower overpotentials than the polished electrode in the range studied. This may be due to the fact that they had larger actual surface areas, and thus lower local current densities.

At low current densities ($<10 \text{ mA/cm}^2$), the pyramidal and the grooved electrodes also had overpotentials lower than those of the polished electrode because of their larger surface area. However, at higher current densities, their overpotentials became higher than those of the group (1) electrodes----the polished and the sanded ones. This may be explained by the differences in current distribution, which is characterized by the Wagner number, $W = Kb/LJ$, in the Tafel Region. The larger the Wagner number is, the more uniform the current distribu-



XBL 806-10312

FIGURE (29) HYDROGEN OVERPOTENTIALS ON NICKEL ELECTRODES OF DIFFERENT SURFACE MORPHOLOGIES.

TABLE (2) SUMMARY OF THE POLARIZATION PARAMETERS

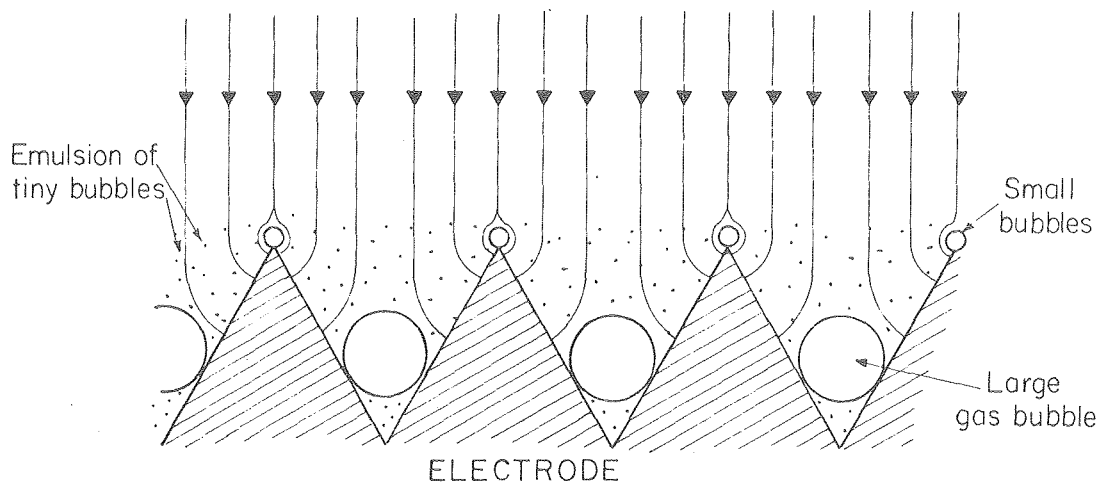
ELECTRODE	REGION (1)			REGION (2)		
	CURRENT DENSITY	a	b	CURRENT DENSITY	a	b
POLISHED 	0.4 mA/cm ² TO 2,000 mA/cm ²	-0.46V	0.086V	-	-	-
SANDED 	0.4 mA/cm ² TO 20 mA/cm ²	-0.40V	0.071V	40 mA/cm ² TO 2,000 mA/cm ²	-0.46V	0.111V
GROOVED 	1 mA/cm ² TO 10 mA/cm ²	-0.48V	0.100V	10 mA/cm ² TO 1,000 mA/cm ²	-0.60V	0.167V
PYRAMIDAL 	1 mA/cm ² TO 10 mA/cm ²	-0.50V	0.100V	10 mA/cm ² TO 1,000 mA/cm ²	-0.58V	0.145V
LITERATURE VALUES ¹⁹	a = -0.55 to -0.72V ; b = 0.10 to 0.14V					

tion will be. In systems of identical geometry, the current distribution depends only on Kb/J . At higher current densities, since W is smaller, the current distribution tends to be less uniform. For the group (1) electrodes, J is slightly higher along the edges. However, the case is more serious for the group (2) electrodes. (See Figure (30).) The current density will be higher on the ridges and the apexes. The fraction of current distributed along these sites increased as current density is increased. In addition, usually, more bubbles are nucleated in the troughs than on the ridges and the apexes. After molecular hydrogen is liberated in regions of high current density, it diffuses to the active nucleation sites and desorbs into the gas phase. Thus, the trough bubbles can grow to larger sizes. These large bubbles cause higher resistance for current to flow into the troughs. Hence, more current will be concentrated at the ridges and the apexes than in the case without bubbles. The resulting higher local current density will cause higher overpotential.

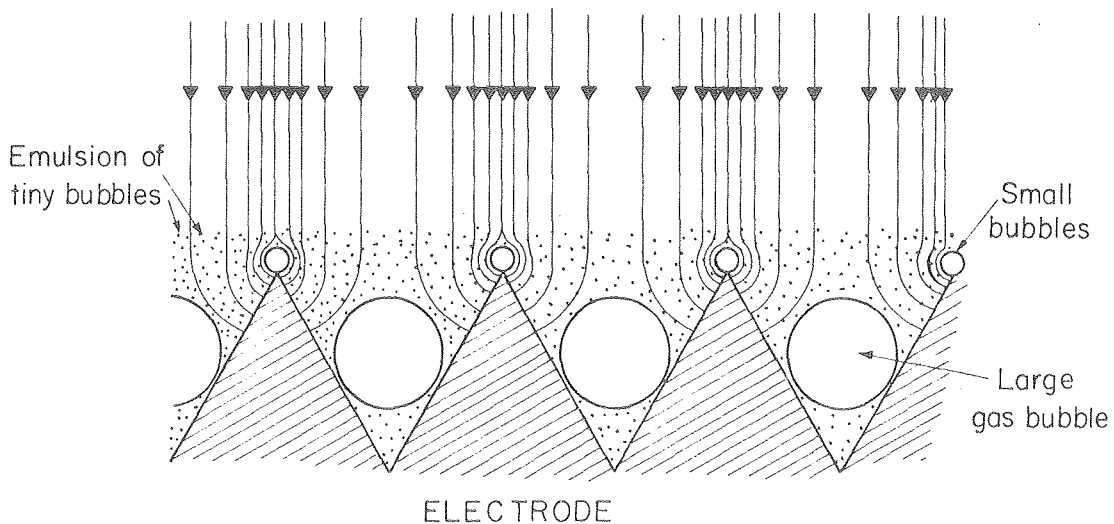
(ii) In Forced Flow

To detect any effects of forced flow on the polarization behavior, the difference between overpotentials on group (1) electrodes: $(\eta)_{\text{flow}} - (\eta)_{\text{stagnant}}$, is plotted against current density. The results are shown in Figure (31).

It is seen that forced flow decreases the overpotential only in the lower current density region. The lower the current density, the more the overpotential is decreased. Also, the extent of the reduction of the overpotential depends directly on the flow rate. That the flow affects the overpotential more at lower current densities may be explained by the enhancement of mass transfer caused by the mechanical stirring of the bubbles. At low current densities, the bubbles are so few and so small that the solution is not stirred effectively by bubbles. Therefore, in this region, forced flow improves mass transfer, resulting in a decrease in concentration overpotential. As the current density is increased, the bubbles become larger in size and increase in number. Their rising velocities become higher. They stir up the electrolyte and decrease the concentration overpotential. Thus the effect of the forced flow becomes negligible as the rate of generation of bubbles increases.



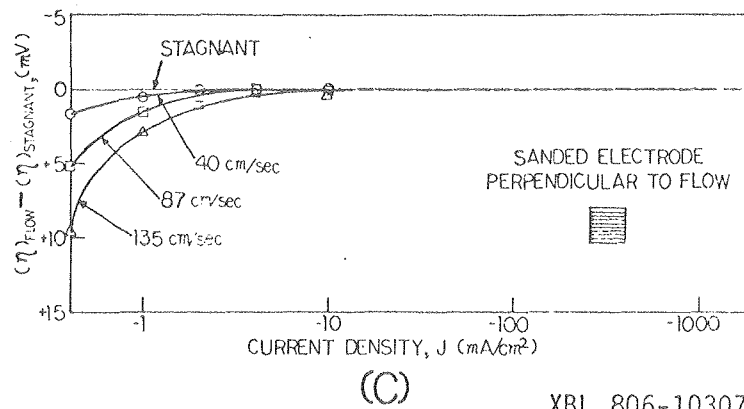
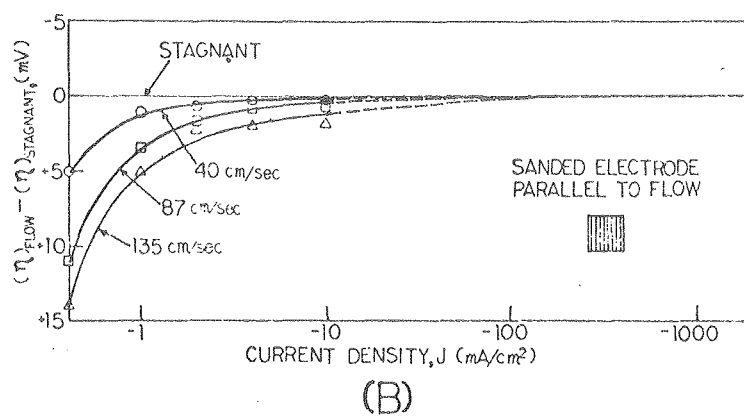
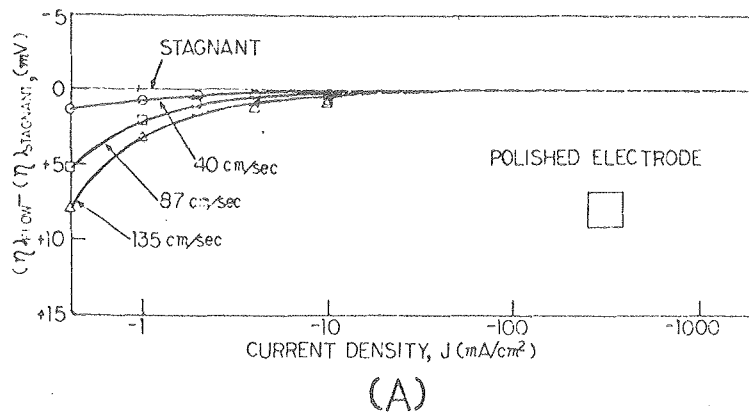
(A) Low Current Density



(B) High Current Density

XBL 808-5630

FIGURE (30) SCHEMATICS OF THE CURRENT DISTRIBUTION ON THE GROUP (2) ELECTRODES.



XBL 806-10307A

FIGURE (3I) REDUCTION OF OVERPOTENTIAL CAUSED BY FORCED FLOW

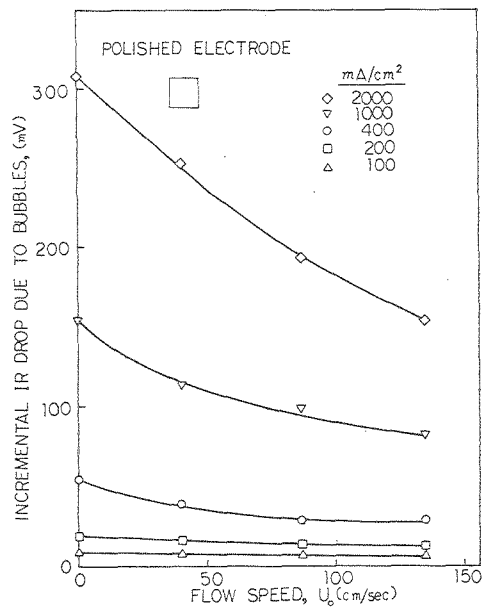
The effect of the forced flow on overpotential varies with the surface morphology of the electrode. Forced flow was found more effective in reducing the overpotential for the parallel sanded electrode than for the others. Comparison between the two sanded electrodes implies that the stirring action of forced flow is able to penetrate closer to the surface when the sanded grooves are parallel to the flow. Therefore, in the latter case, the forced flow reduces the concentration difference and the bubble entrapment more effectively. Since the polished electrode has no bubbles entrapped, the only effect of the flow is to reduce the concentration difference of dissolved gas. Hence, the magnitude of the reduction of the overpotential is smaller than in the case of the parallel sanded electrode.

(2) Ohmic Drop & Resistance Measurements

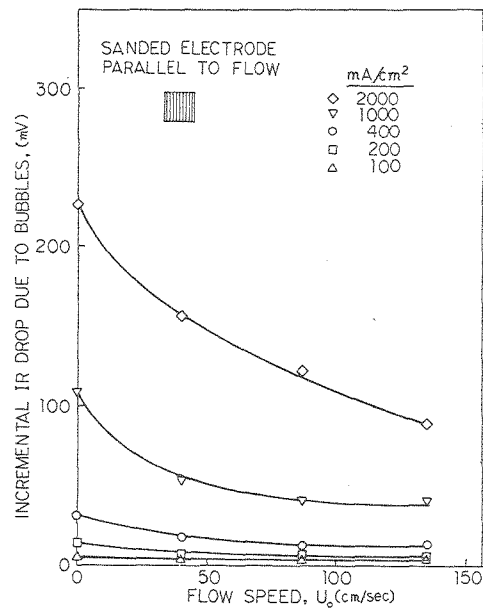
(i) Incremental Ohmic Drop Caused By Bubbles, ΔIR

The effect of flow on ohmic resistance was also found to be quite different for the two groups of electrodes. The incremental ohmic drop caused by bubbles, ΔIR , is plotted vs the flow rate in Figure (32) and (33) for the group (1) and the group (2) electrodes, respectively. As expected, the incremental ohmic drop increases with current density, and decreases with flow rate. By comparing Figures (32) and (33), it is evident that at any given current density the magnitude of the incremental ohmic drop for the group (2) electrodes is several times higher than those for the group (1) electrodes. Also, the reduction of the incremental ohmic drop by the flow is less effective for the group (2) electrodes.

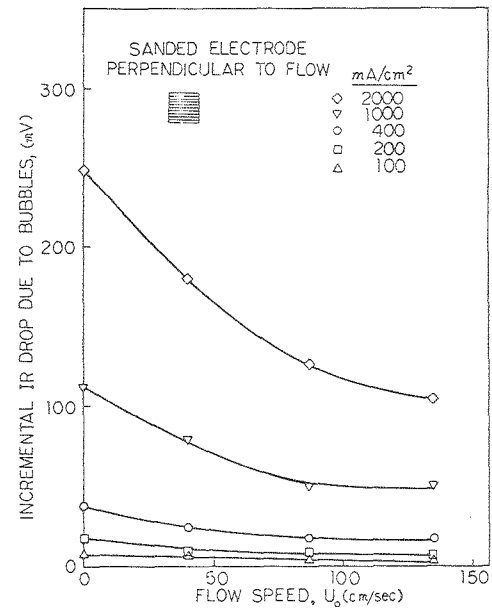
(ii) Incremental Resistance Caused By Bubbles, ΔR_b



(A)



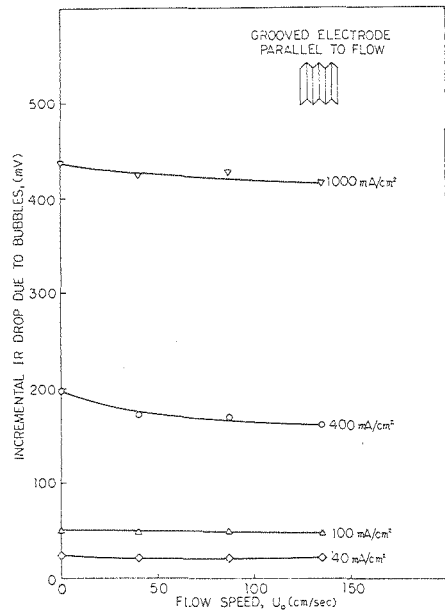
(B)



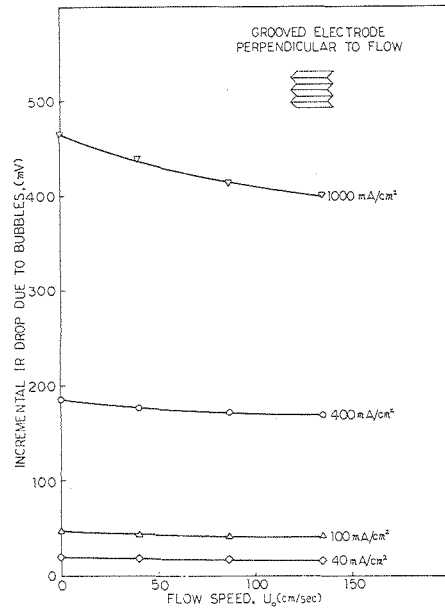
(C)

XBL 806-10419A

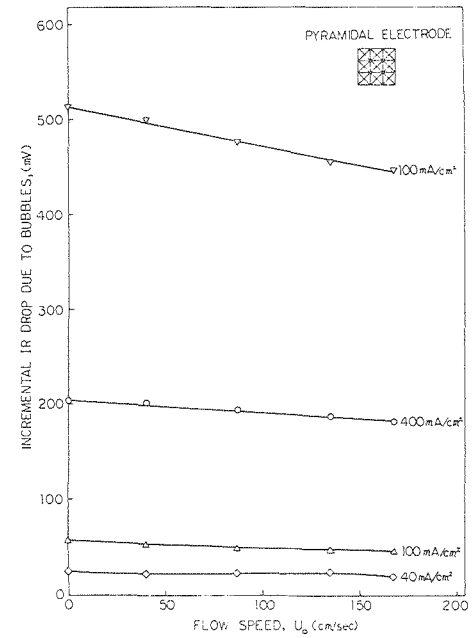
FIGURE (32) INCREMENTAL OHMIC DROPS CAUSED BY BUBBLES VS FLOW VELOCITY FOR GROUP (I) ELECTRODES.



(A)



(B)



(C)

XBL 806-10311A

FIGURE (33) INCREMENTAL OHMIC DROPS CAUSED BY BUBBLES VS FLOW VELOCITY FOR GROUP (2) ELECTRODES.

The effects of current density, flow rate, and surface morphology on the incremental ohmic resistance is discussed in the following sections. A summary of the incremental resistance data is listed in Table (3). To allow analysis of the effect of gas bubbles on cell performance, it is better to evaluate the behavior of incremental ohmic resistance, rather than that of incremental ohmic potential drop. The incremental potential drop has a much larger range, corresponding to the large range of current densities covered.

(a) Group (1): Polished and Sanded Electrode

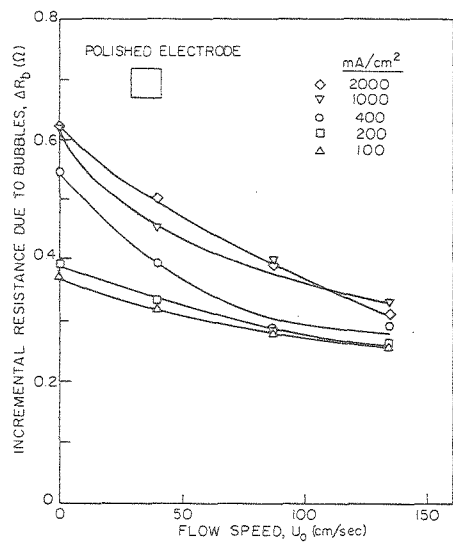
The incremental resistances caused by bubbles are plotted in Figure (34) for the group (1) electrodes. For all of the electrodes in group (1), the incremental resistance increased with increasing current density and decreased with increasing flow rate. The percentage of the reduction of ΔR_b by forced flow changes with current density. For a fixed current density, the reduction percentage is not proportional to the magnitude of the forced flow. Instead, the additional reduction gained by increasing the flow rate decreases as the flow rate becomes too high. Also, the reduction of ΔR_b by a fixed forced flow is larger for a higher current density. Since forced flow requires additional energy consumption, we have to pay very careful attention in choosing the right flow rate.

The three electrodes respond to the effects of current density and forced flow to different degree according to their surface morphologies. Under the same conditions, the parallel sanded electrode usually has the smallest incremental resistance; whereas the polished electrode has the largest one. These trends are very similar to those concerning bubble size. This suggest that the incremental resistance depends strongly on bubble size. Actually, it is possible to propose a model to predict ΔR_b based on the bubble size. A detailed discussion of this model will be given in the Appendix.

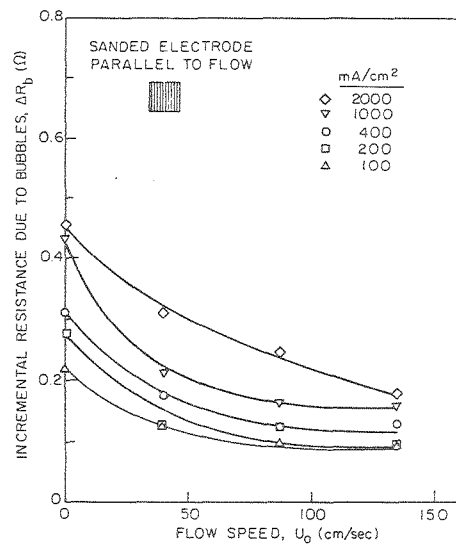
Figure (35) shows clearly that there is a linear correlation between the incremental resistance and the current density on a log-log plot, for each flow rate. Also, the higher the flow rate, the lower is ΔR_b . It seems that it may be possible to correlate the effects of the flow rate and the current density by proper analysis.

TABLE (3) SUMMARY OF THE INCREMENTAL RESISTANCE BEHAVIORS OF THE VARIOUS ELECTRODES

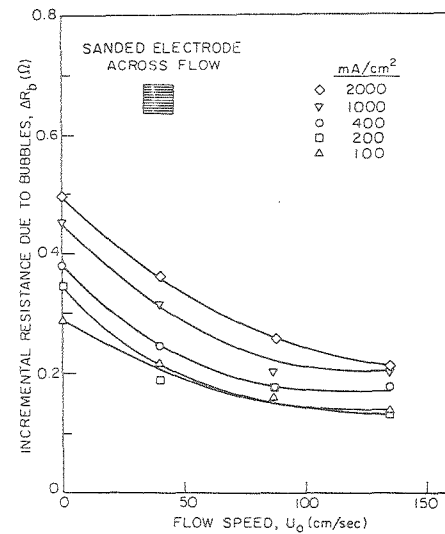
CONDITIONS	<u>NORMALLY BEHAVING GROUP</u> POLISHED & SANDED ELECTRODES	<u>STRANGELY BEHAVING GROUP</u> GROOVED & PYRAMIDAL ELECTRODES
INCREASING CURRENT DENSITY	INCREASING ΔR_b	DECREASING ΔR_b
INCREASING FLOW RATE	DECREASING ΔR_b	DECREASING ΔR_b (TO A LESS EXTENT)
COMPARISON BETWEEN THE TWO GROUPS.	GROUP (1) < GROUP (2) (0.1 - 0.6 Ω) (2.6 - 1.6 Ω)	
COMPARISON BETWEEN THE ELECTRODES IN ITS OWN GROUP		



(A)



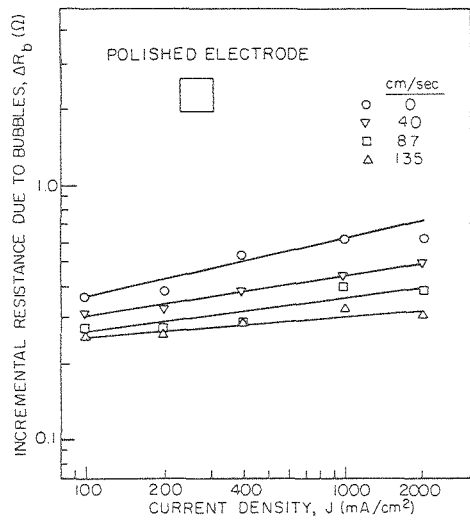
(B)



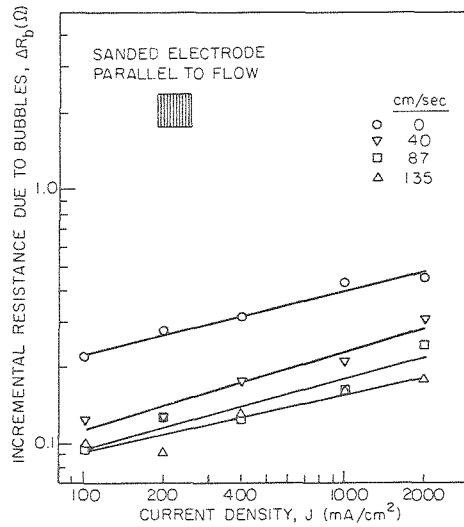
(C)

XBL 804-5039A

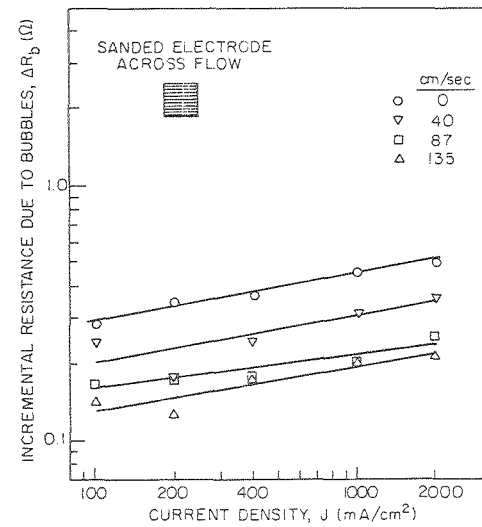
FIGURE (34) INCREMENTAL RESISTANCE CAUSED BY BUBBLES VS FLOW VELOCITY FOR GROUP (I) ELECTRODES.



(A)



(B)



(C)

XBL 804-5036B

FIGURE (35) INCREMENTAL RESISTANCE CAUSED BY BUBBLES VS CURRENT DENSITY FOR GROUP (I) ELECTRODES.

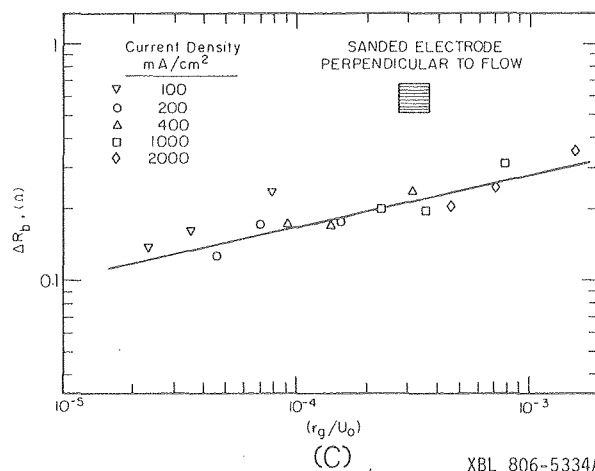
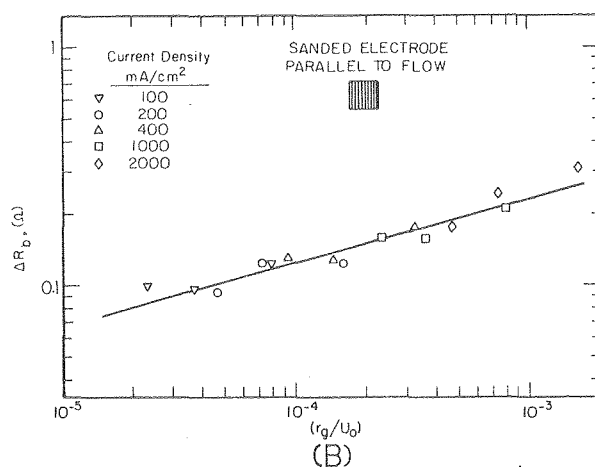
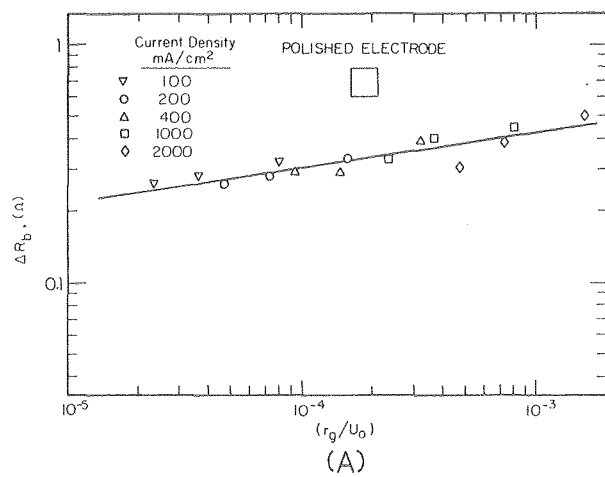
Let us start the analysis by looking at the factors that determine the magnitude of ΔR_b . It is obvious that ΔR_b should depend strongly on the gas layer thickness, X . In the Appendix, it is shown that ΔR_b should be proportional to X . The gas layer thickness should increase with the rate of generating gas, r_g ($\text{cm}^3/\text{sec}\cdot\text{cm}^2$), which can be calculated from the current density. If a forced flow is applied to remove the gas bubbles from the electrode surface, a thinner gas layer will be resulted. The higher the flow velocity, U_o (cm/sec), is, the thinner the gas layer will be. Therefore, it seems that X should be a function of the dimensionless ratio (r_g/U_o). Since, ΔR_b is proportional to X , ΔR_b should also depend on (r_g/U_o).

Figure (36) shows the plots of ΔR_b vs (r_g/U_o) for each of the group (1) electrodes in a log-log plot. All the data are found to fall on a single straight line. Again, the polished electrode lies highest, whereas the parallel sanded electrode is the lowest. The slopes and intercepts of these lines are listed in Table (4).

The significance of Figure (36) is that it helps to choose the appropriate flow rate for a specific current density. The plots provide us the correlations between ΔR_b , r_g and U_o . If the current density is chosen, these correlations can be used to determine how ΔR_b , and thus the reduction of cell voltage, changes with the flow rate. If the energy consumption of forced flow is known, it is very easy to find the appropriate flow rate that will provide the lowest energy consumption.

Let us now make a rough estimate of how these results could be used in engineering application. Often the electrodes used are smooth, even polished. If the system is operated under an appropriate forced flow rather than in stagnant solution, the incremental resistance caused by bubbles can be reduced by 30-45 %. If the polished electrodes are replaced by electrodes sanded with 100 grit sandpaper parallel to the flow, the incremental resistance will be reduced by 30-45 % in stagnant electrolyte, or 70-80 % under an appropriate forced flow. In the latter case the reduction will correspond to a few percent of the total energy requirement. The actual percentage will depend on the cell design and the applied current density.

(b) Group (2): Grooved and Pyramidal Electrodes



XBL 806-5334A

FIGURE (36) THE DEPENDENCE OF ΔR_b ON r_g AND U_0 .

TABLE (4) SUMMARY OF THE DEPENDENCE OF ΔR_b ON (r_g/U_0)

ELECTRODE	INTERCEPT	SLOPE	CORRELATION
POLISHED ELECTRODE 	0.55	0.15	$\Delta R_b = 3.56(r_g/U_0)^{0.15}$
PARALLEL SANDED ELECTRODE 	0.18	0.27	$\Delta R_b = 1.53(r_g/U_0)^{0.27}$
CROSSWISE SANDED ELECTRODE 	0.33	0.20	$\Delta R_b = 2.14(r_g/U_0)^{0.20}$

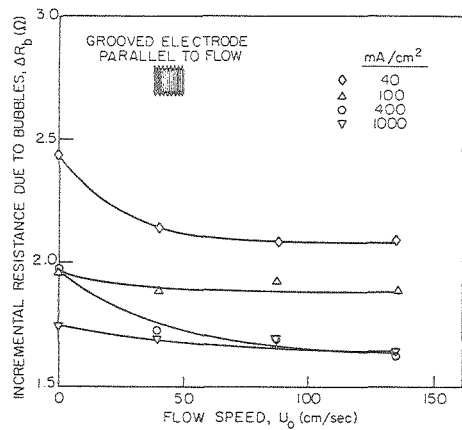
The incremental resistance behavior for these electrodes is quite strange. Results are plotted in Figure (37) for the group (2) electrodes.

First, the incremental resistance decreases as the current density is increased. This is in quite a contrast to results obtained on group (1) electrodes. One possible reason may be that the current distribution is different in various current density regimes. As shown schematically in Figure (30), the current should become more concentrated along the ridges of the grooves or at the apexes of the pyramids as the current density is increased. As observed usually, for the pyramidal electrode and the parallel grooved electrode, most of the gas bubbles are generated in the troughs and mostly move within there. In the range studied, the increase, with current density, of the rate of generating gas was smaller along the ridges and on the apexes than in the troughs. However, as the current density is increased, a larger fraction of current is concentrated in regions where the resistance offered by bubbles is smaller. This may be at least a partial explanation for why the incremental resistance decreased as the current density was increased.

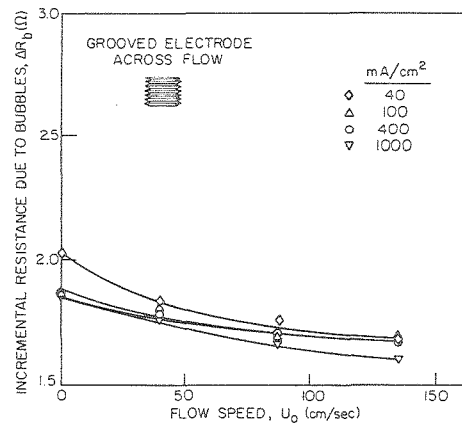
For the crosswise grooved electrode, all the bubbles generated in the troughs have to come out of the grooves and float up along the surface of the electrode. The gas content along the top of the peaks would then increase with the current density. Therefore, the extent of reduction of the incremental resistance with the current density should be smaller. In fact, this is what is shown in Figure (37)(B).

The effect of flow on the incremental resistance for group (2) electrodes is very similar to that found for group (1) electrodes; the incremental resistance decreases as the flow rate increases. However, the degree of reduction of the incremental resistance is much smaller. This may be due to the fact that usually the flow could remove the bubbles near protrusions but not those in the troughs. Therefore, the fraction of bubbles removed by the flow appears to be smaller for group (2) electrodes.

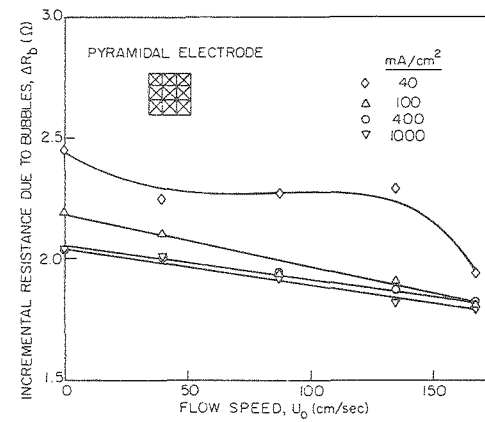
By looking at the families of curves in Figure (37), we can tell that the crosswise grooved electrode demonstrates the lowest incremental resistance, and the pyramidal electrode the highest. One of the reasons for the crosswise grooved electrode yielding the lowest incremental resistances may be that the bubbles in the troughs can be stirred up and "kicked out" of the grooves more easily in the high current density range.



(A)



(B)



(C)

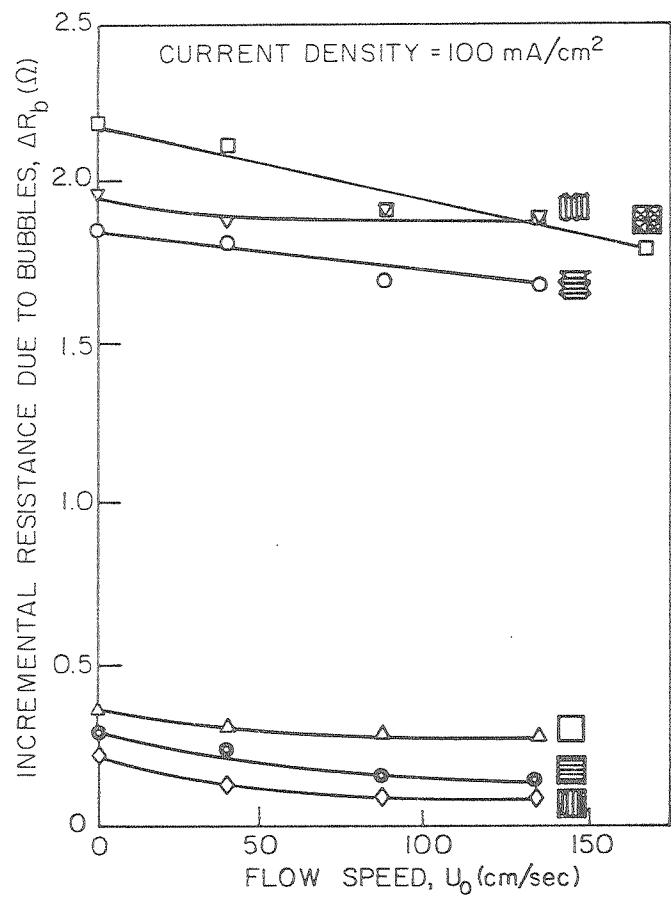
XBL 804-5041A

FIGURE (37) INCREMENTAL RESISTANCE CAUSED BY BUBBLES VS FLOW VELOCITY FOR GROUP (2) ELECTRODES.

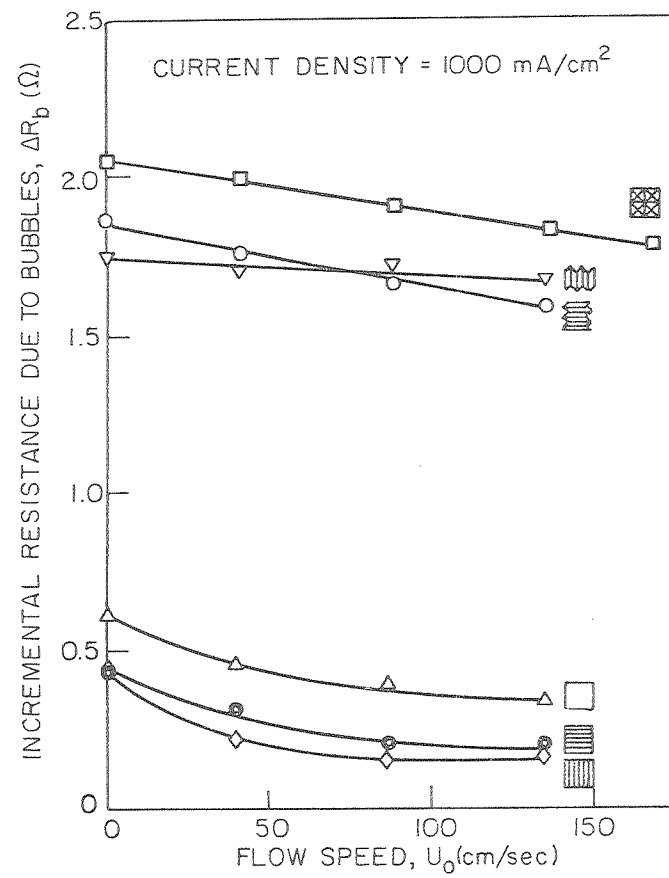
(c) Comparison Between The Two Groups Of Electrodes

In comparing the incremental resistances for the two groups of electrodes (see Figure (38)), it is very obvious that the incremental resistances for the group (2) electrodes are several times higher than those for the group (1) electrodes. A contributing factor may be that the group (2) electrodes had a large number of very tiny bubbles in emulsion filling up the spaces left by the big bubbles. The resulting resistance could be fairly high.

The differences between the incremental resistances for the two groups of electrodes decreases with increasing current density (compare Figures (38)(A) and (38)(B)). This is because the effect of the current density on the incremental resistances is in opposite direction for the two groups of electrodes.



(A)



(B)

XBL804-5045A

FIGURE (38) COMPARISONS BETWEEN THE INCREMENTAL RESISTANCES OF GROUP (1) AND GROUP (2) ELECTRODES.

(V) MISCELLANEOUS

(1) The Dominating Role of Nucleation Site Distribution and Current Distribution in Bubble Formation

As shown in Chapter (III), the number density and size range strongly depend on the current density. Generally, it was thought that the current distribution was the main factor determining the relative rates of bubble generation on the electrode. However, in this study, it has been found that the distribution of the nucleation sites, rather than the macroscopic current distribution, is the dominant factor affecting bubble evolution.

On the grooved and pyramidal electrodes used in this study, various nucleation sites were created by the mechanical cutting. The most active sites in generating gas bubbles were the troughs. According to Wagner's analysis²⁰, the bottoms of the troughs are supposed to have the lowest current density. It is well known that cracks or cavities are active nucleation sites for gas bubble formation in the liquid phase, as in boiling^{21,22}. This suggests that the electrolytic gas bubble evolution might be dominated by the nucleation site density rather than by the primary electric field.

In an attempt to illustrate what role current distribution could play in bubble formation, a special experiment was performed to generate hydrogen under the condition of non-uniform current distribution. The same flow channel was employed, but one of the anodes was disconnected from the power supply (see Figure (39)(A)). In this case, the current density on the cathode should be much higher near the working anode than near the disconnected anode. The cathode used was the polished electrode. Experiments were carried out at current densities of 4.6 mA/cm², 100 mA/cm², and 1,000 mA/cm² in stagnant electrolyte. In previous experiments with uniform current distribution, this cathode had uniform nucleation site distributions at these current densities. If the gas evolution behavior is determined by the primary field, a very non-uniform gas bubble layer should form on the cathode. In addition, this non-uniformity should increase as current density is increased, because the current distribution is less uniform at

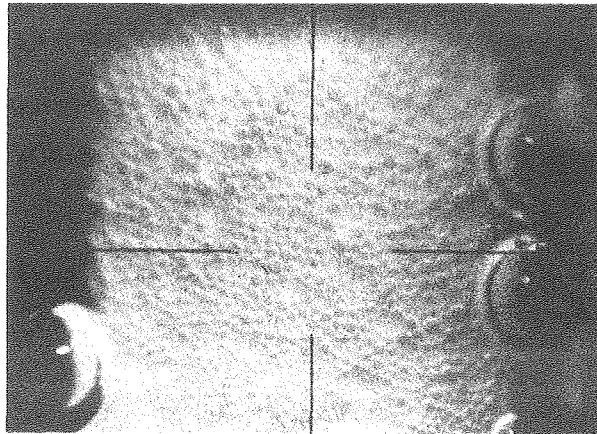
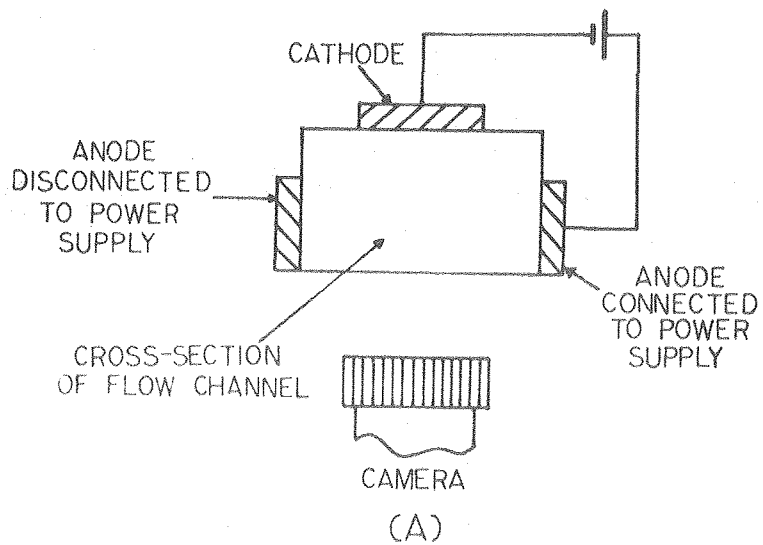


FIGURE (39) (A) SCHEME FOR THE ELECTRIC CIRCUIT OF THE NON-UNIFORM CURRENT DISTRIBUTION EXPERIMENT.

(B) PHOTOGRAPH OF THE BUBBLE FORMATION AT 1 A/cm^2 IN THE NON-UNIFORM CURRENT DISTRIBUTION EXPERIMENT.

XBB-800-12057

higher current density. However, it was found that the bubble distributions were uniform at all three current densities. (Figure (39)(B) shows an example of this phenomenon at 1,000 mA/cm².) We therefore conclude that the behavior of hydrogen evolution is dominated by the nucleation site distribution and that the impedance offered by the bubble layer, in serve with the bulk electrolyte farther away from the electrode, shifts the current distribution towards uniformity.

(2) The Dependence of Cell Voltage on the Specific Surface Area and Surface Morphology of the Electrode

In Kuhn, Yusof and Hogan's study regarding electrode structure and surface texture in the performance of gas evolving electrodes¹⁵, they concluded that substantial voltage reductions can be obtained by using multiplex electrode structure because of the increase in specific surface area. It is obvious that a reduction in overpotential is caused by a decrease in current density. However, it is rather doubtful whether a reduction in cell voltage will result whenever there is an increase of the specific area.

The cell voltage is dependent on both the overpotential and the ohmic drop. The ohmic drop is determined by the bubble evolution behavior, which is closely related to the surface morphology, especially the active nucleation site distributon. Certain types of surface morphologies have large specific surface areas, but provide relatively few active nucleation sites and/or unfavorable nucleation site distribution. This may cause higher incremental resistance resulting in a higher overall cell voltage. The grooved and the pyramidal electrodes are good examples. These electrodes have specific surface areas twice as large as that of the polished electrode. However, the incremental ohmic drops of the former ones are noticable higher than the latter ones. (See Figure (38).)

According to Kuhn, Yusof and Hogan's data¹⁵, sheet electrodes with very high specific surface areas give significantly higher overvoltages than electrodes of lower specific areas. Kuhn et al explains this in terms of bubble entrapment. Taking a careful look at their SEM

photographs, one can easily see that the various electrodes have differing surface features. The ones that have a high density of uniformly distributed nucleation sites (cracks or cavities in these cases) operate with lower cell voltages (i.e. the one polished with C600 grade emery paper and the one etched in 6M sulfuric acid for 5 minutes).

Therefore, in order to reduce the cell voltage by manipulating the surface morphology, we have to consider not only the specific surface area but also the number density and distribution of nucleation sites created.

(3) The Dependence of the Incremental Resistance on the Height of the Electrode

As mentioned in Chapter (III), gas bubbles become larger as they rise up along the electrode because of scavenging action (coalescence) and absorbing gas from the supersaturated electrolyte. Hence, at a fixed current density, the average bubble layer thickness will be larger for a taller electrode. The resulting ΔR_b will then be higher. However, this assumption holds only up to certain point, because the bubble sparging phenomenon changes as the electrode height is increased. The specific height at which upward sliding bubbles separate from the electrode should depend on the cell design, especially the gap width, on current density, and on flow rate. Nevertheless, this assumption should hold within our experimental conditions. Since the electrode height is fixed in our system, a separated simple experiment was performed to demonstrate this phenomenon. It was carried out with a simple cell containing two parallel polished nickel electrodes (3 cm \times 1.5 cm) set 1 cm apart, cast in Teflon (see Figure (40)). These electrodes were so constructed that by simply turning the cell by 90°'s, their heights could be set at either 3 cm or 1.5 cm. The experiment was carried in a 5M KOH bath. The current applied was 2A, corresponding to a current density of 444 mA/cm². Cell voltage were measured 20 minutes after the current was applied. The results are listed in Table (5). The cell voltages were lower for the runs with 1.5 cm high electrode. Since in all the experimental runs the electrodes had the same areas and the same gap widths, the differences in cell voltages had to be due to the differences in incremental ohmic drops. We can therefore conclude that the height of the electrode is one of the factors affecting the incremental resistance.

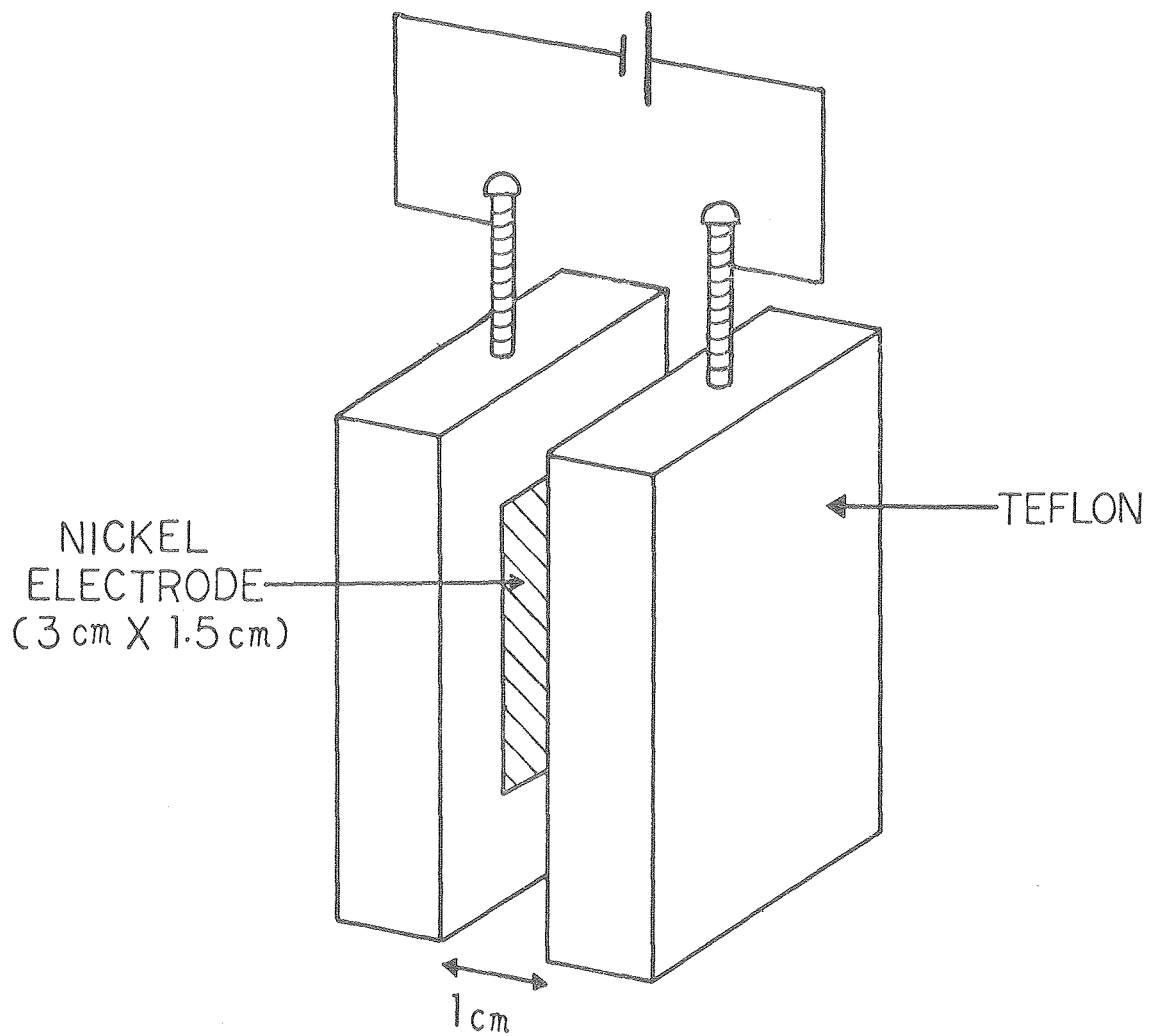


FIGURE (40) SKETCH OF THE CELL IN THE EXPERIMENT WITH DIFFERENT ELECTRODE HEIGHTS.

XBL 8010-12585

TABLE (5) CELL VOLTAGES FOR THE ELECTRODES WITH DIFFERENT HEIGHTS

ELECTRODE	CELL VOLTAGE
 <p data-bbox="483 1014 646 1182">3 CM HIGH X 1.5 CM WIDE</p>	<p data-bbox="1000 821 1101 1115">3.36 V 3.38 V 3.36 V 3.36 V 3.34 V</p>
 <p data-bbox="467 1587 646 1755">1.5 CM HIGH X 3 CM WIDE</p>	<p data-bbox="1000 1461 1101 1629">3.27 V 3.27 V 3.27 V</p>

(VI) CONCLUSIONS

The principal conclusions of this work can be summarized as follows :-

- (1) Hydrogen bubble evolution behavior strongly depends on the surface morphology of the cathode.
- (2) The dominant factors affecting bubble evolution behavior are the density and the distribution of the nucleation sites.
- (3) The polarization behavior is heavily influenced by the surface morphology of the electrode. Among the electrodes studied, the sanded electrodes demonstrated the lowest overpotentials.
- (4) The orientation of the surface morphology to the flow has no significant effect on the mass transfer and charge transfer overpotentials.
- (5) Forced flow can reduce the mass transfer overpotential only at low current densities ($< 10 \text{ mA/cm}^2$). The reduction increases with increasing flow rate and decreasing current density. Within our experimental range, the reduction is around a few mV to 14 mV. It is the highest for the parallel sanded electrode.
- (6) Incremental resistance caused by bubbles increases with the average bubble size at separation.
- (7) For the sanded and the polished electrodes, both the incremental resistance and the bubble size increase as current density is increased. The incremental ohmic drop becomes significant only at current density higher than 40 mA/cm^2 . Usually, the incremental resistances are around a few tenths of an ohm. The corresponding incremental ohmic drops will then range from a few mV (at 40 mA/cm^2) to $\sim 200\text{-}300 \text{ mV}$ (at 2 A/cm^2).
- (8) Both incremental resistance and bubble size are reduced by forced flow. The degree of reduction of the incremental resistance decreases as the flow rate is increased to high values. Therefore, depending on the current density, the forced flow can reduce the incremental resistance effectively only up to certain flow velocity. For the sanded and the polished electrodes, the reduction ranges from 30-55 %.

- (9) The incremental resistance is found to be dependent on the dimensionless ratio of the specific rate of bubble evolution and the velocity of the forced flow, (r_g/U_o).
- (10) Incremental resistance and bubble size are strongly affected by the surface morphology of the electrode. In this study, the lowest incremental resistance and bubble size were found on electrodes which were sanded parallel to the direction of flow.
- (11) The number of nucleation sites activated increases as current density is increased; it levels off at around a few hundred mA/cm².
- (12) The effect of forced flow on cell voltage varies with current density. Forced flow reduces the mass transfer overpotential noticeable only at low current densities (< 10 mA/cm²), and decreases the incremental ohmic drop only at high current densities. It is much less effective in reducing the cell voltage in the transition current density range (~ 10 -40 mA/cm²).

APPENDIX

(A-1) MODELLING FOR THE INCREMENTAL RESISTANCE CAUSED BY BUBBLES, ΔR_b

As shown in the preceding chapters, for the normally behaving electrodes, both the bubble size and ΔR_b increase with current density, and decrease with flow rate. Therefore, it should be possible to derive a model to describe how the resistance is increased by the bubbles as a function of the bubble size. First, we will discuss a model for the ideal case, involving uniform bubbles, proposed by P. Sides²³. Then, we will modify this ideal model to fit the phenomena observed more closely.

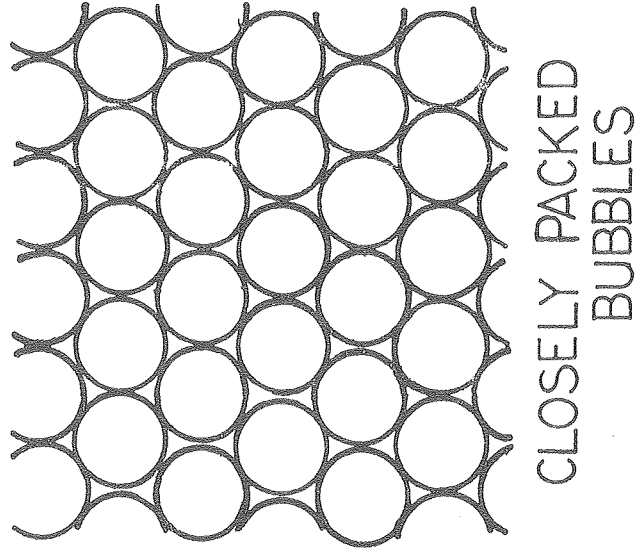
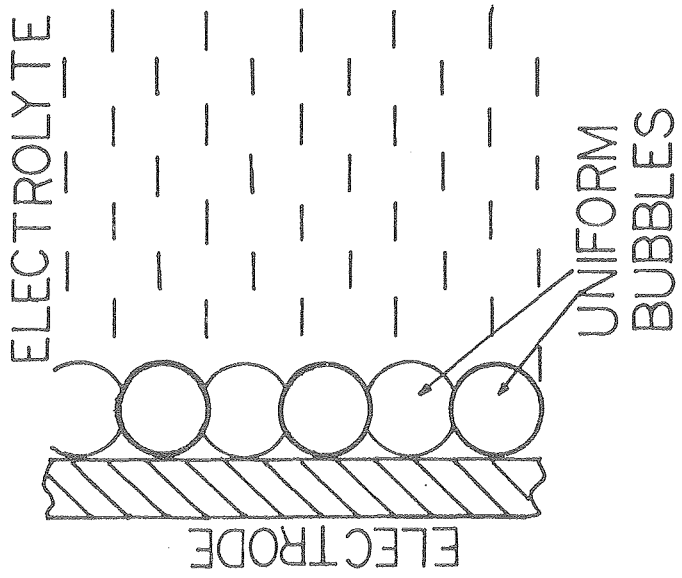
(1) The Sides Model for Uniform Bubble Size

In part of Sides' work, he assumes that all the bubbles on an electrode are uniform spheres with diameter D , and they are hexagonally closely packed. (See Figure(A-1) (A) & (B).) In deriving the model, Sides started with an electrode of area A in an electrolyte of conductivity K without gas bubbles (Figure (A-2)(A)). In this case, the resistance between the electrode and a point P would be R_{ng} . If a section of electrolyte of thickness D was removed from the electrode (Figure (A-2)(B)), the new resistance of the electrolyte section would be $(R_{ng} - D/AK)$. The next step was to refill the empty section with closely packed bubbles (with uniform diameters D) and electrolyte, as shown in Figure (A-2)(C). The resistance of this refilled section should be (D/AK_g) ; where K_g was the effective conductivity of this section. Therefore, the total resistance of electrolyte with gas bubble becomes:

$$R_g = R_{ng} - D/AK + D/AK_g \quad \text{(A)(1)}$$

Since $\Delta R_b = R_g - R_{ng}$ _____ (5)

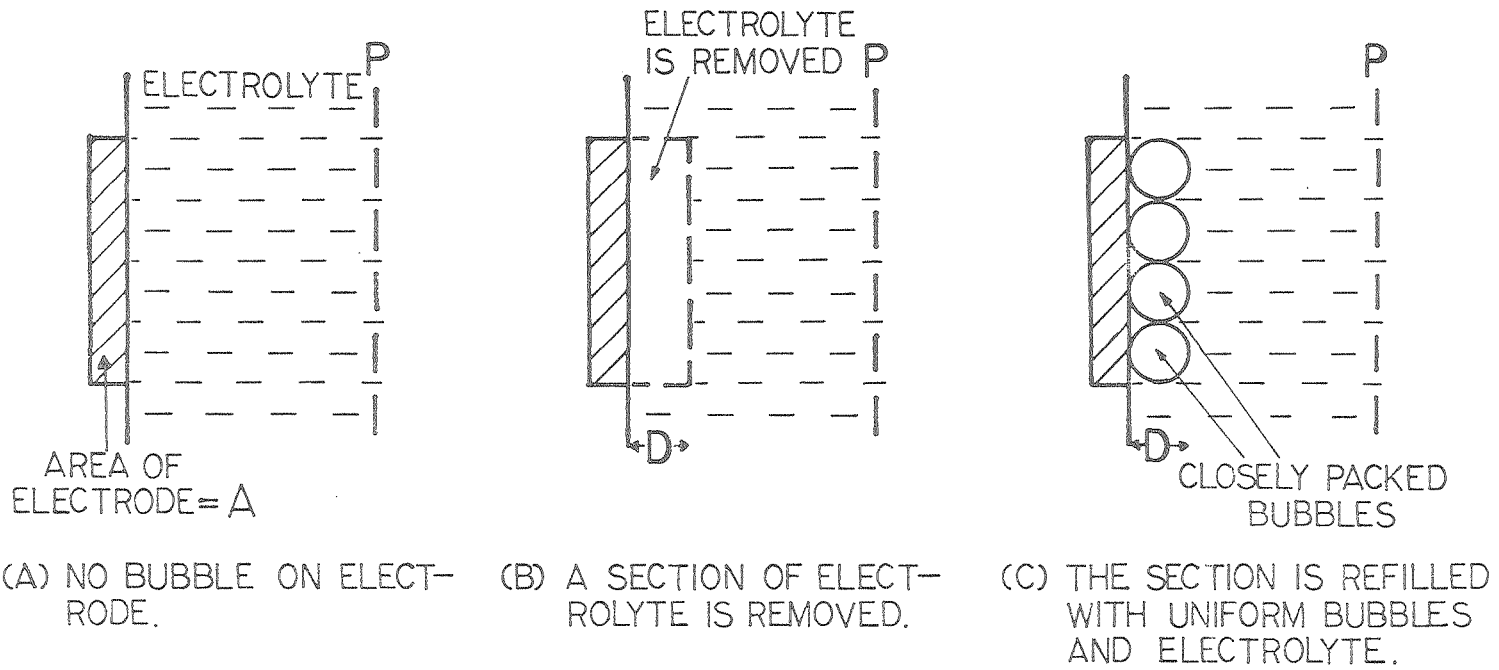
therefore $\Delta R_b = D/AK_g - D/AK$
 $= (D/A)(1/K_g - 1/K)$ _____ (A)(2)



(A) SIDE VIEW (B) FRONT VIEW

XBL 806-10315

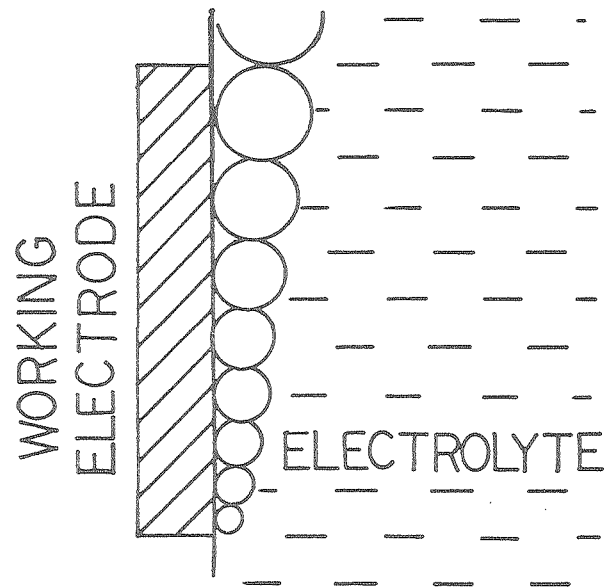
FIGURE (A-1) GEOMETRY OF SIDES' MODEL



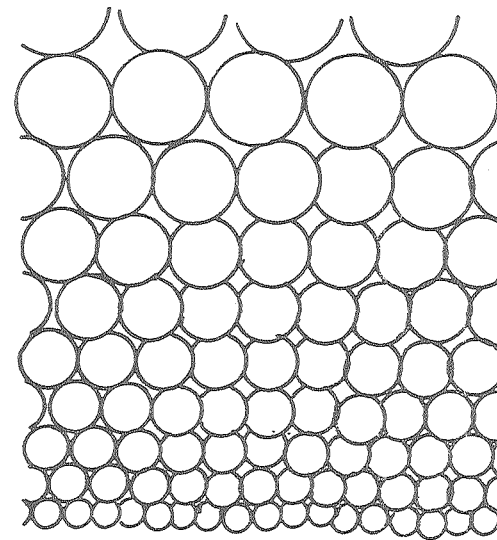
XBL 806-10316

FIGURE (A-2) SCHEMES FOR DERIVING THE SIDES' MODEL.

(A) SIDE VIEW



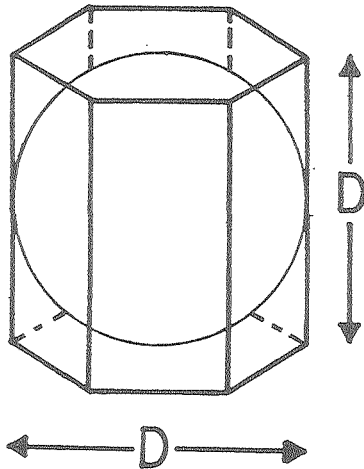
(B) FRONT VIEW



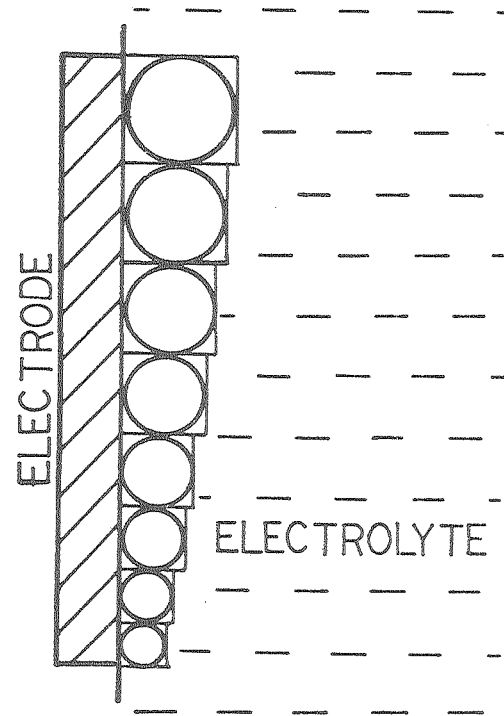
XBL 806-10313

FIGURE (A-3) ROUGH SKETCHES FOR THE BUBBLE FORMATION IN A REAL ELECTROLYTIC SYSTEM.

(A) EACH BUBBLE IS TREATED AS A SINGLE HEXAGONAL CELL.



(B) BUBBLES ARE TREATED AS PARALLEL HEXAGONAL UNIT CELLS ON THE ELECTRODE.



XBL 806-10314

FIGURE (A-4) SCHEMES FOR TREATING THE BUBBLES AS HEXAGONAL UNIT CELLS IN DEFINING THE AVERAGE GAS LAYER THICKNESS, X .

Table (A-1) shows the comparison of sample experimental data and calculated values. The deviation of calculated values from experimental data in most cases is within $\pm 5\%$, and it never exceeds $\pm 10\%$. Considering the random nature of bubble nucleation and growth, plus the inaccuracies involved in the measurements, the theoretical results based on a simple model are in reasonably agreement with the experimental data.

TABLE (A-1) COMPARISON OF THE EXPERIMENTAL- AND THE CALCULATED ΔR_b 'S

ELECTRODE	CURRENT DENSITY	FLOW VELOCITY	EXPERIMENTAL $(\Delta R_b)_{exp}$	CALCULATION BASED ON THE MODEL	
				X	$(\Delta R_b)_{cal}$
	1,000 mA/cm ²	0	0.616	235 μ m	0.588 (I.E. (0.95) $(\Delta R_b)_{exp}$)
	1,000 mA/cm ²	0	0.432	177 μ m	0.442 (I.E. (1.02) $(\Delta R_b)_{exp}$)
	1,000 mA/cm ²	40cm/SEC	0.212	92.4 μ m	0.231 (I.E. (1.09) $(\Delta R_b)_{exp}$)
	1,000 mA/cm ²	0	0.448	180 μ m	0.449 (I.E. (1.002) $(\Delta R_b)_{exp}$)

LIST OF SYMBOLS

- a = a constant in the Tafel Relation
- A = the area of the electrode
- b = the Tafel slope for the overpotential curve
- D = the thickness of a section of electrolyte
- ΔE = the equilibrium potential difference between the working electrode and the reference electrode
- I = current
- IR = ohmic voltage drop
- ΔIR = the incremental ohmic drop caused by bubbles
- J = current density
- K = the conductivity of the electrolyte
- K_g = the effective conductivity of the electrolyte filled with gas bubbles
- L = the characteristic length of the electrochemical system
- P = electrical power
- r_g = the rate of generating gas, $\text{cm}^3/\text{sec}\cdot\text{cm}^2$
- R = resistance
- ΔR_b = the incremental resistance caused by bubbles
- Re = Reynolds Number
- R_g = the resistance of the electrolyte containing gas bubbles
- R_{ng} = the resistance of the electrolyte without gas bubbles
- U_o = flow velocity, cm/sec

V = cell voltage

V_m = the measured voltage between the working electrode and the reference electrode

ΔV = the instant voltage drop caused by interrupting the current

W = Wagner Number

= Kb/LJ

X = gas layer thickness

ϵ = gas void fraction

η = the overpotential of the working electrode

ρ = the resistivity of the gas-solution mixture

ρ_0 = the resistivity of the bubble-free solution



= polished electrode



= parallel sanded electrode



= crosswise sanded electrode



= parallel grooved electrode



= crosswise grooved electrode



= pyramidal electrode

ACKNOWLEDGMENT

I wish to express my gratitude to Professor Charles W. Tobias for his direction and encouragement during the course of this work.

This work was supported by the Division of Energy Storage System, Office of Conservation and Solar Energy, U.S. Department, under Contract No. W-7405-Eng-48, through the Chicago Operations and Regional office, Technical management Division, Argonne National Laboratory, Argonne, IL 60439.

REFERENCES

- (1) J.H.Collins, "An Historical View of Developments in Mercury Cell Design and Operation", The Extended Abstracts of the Electrochemical Society, Inc. Spring Meeting, Seattle, Washington, May 1978, Abstrat No.439, P.1101-1103.
- (2) H.W.Schultze, "The Chlorine Industry----Past, Present and Future", The Extended Abstracts of the Electrochemical Society, Inc. Spring Meeting, San Francisco, CA., May 1974, Abstract No.241, P.567-569.
- (3) J.B.Laskin and R.D.Feldwick, "Recent Developments of Large Electrolytic Hydrogen Generators", The Conference Proceedings of the 1st World Hydrogen Energy Conference, Vol.II, P.6B-1 to 6B-20, 1976.
- (4) V.D.Dang, J.Fillo, H.S.Isaacs, O.Lazareth, S.Majeski, H.Makowitz, J.Powell, F.J.Salzano, M.Steinberg and R.Benenati, "Synthetic Fuel Production from Fusion Reactors and High Temperature Electrolysis", Extended Abstracts of the Electrochemical Society, Inc. Spring Meeting, Seattle, Washington, May 1978, Abstract No. 493, P.1233.
- (5) J.B.Bolton, Solid State Chemistry, Vol. 22, P.3-8, 1977.
- (6) S.Das Gupta, H.P.Dhar, j.Jacobs, S.Mohanta, and N.White, "An Electrochemical System for the Production of Hydrogen and Heavy Water from Off-Peak Electricity", Extended Abstracts of the Electrochemical Society, Inc. Spring Meeting, Seattle, Washington, May 1978, Abstract No.495, P.1237.
- (7) p.M.Spaziante, L.Giuffre, A.Nidola, "New Type of Water Electrolyzers for the Production of Large Quantities of Hydrogen", Extended Abstracts of the Electrochemical Society, Inc. Spring Meeting, Seattle, Washington, May 1978, Abstract No.478, P.1194.
- (8) A.P.Fickett and F.R.Kalhammer, "Hydrogen : Its Technology and Implication. Hydrogen Poduction Technology, Vol.I", R.I.Kermode et al., ed. by K.E.Cox & K.D.Williamson, Jr., CRC Pr., Chapter 1, P.3-41, 1977.
- (9) A.J.Appleby, and G.Crepy, "New Developments in Alkaline Electrolysis Technology", Extended Abstracts of the Electrochemical Society, Inc. Spring Meeting, Seattle, Washington, May 1978, Abstract No.485, P.1214.
- (10) D.Landolt, P.Acosta, R.H.Muller, and C.W.Tobias, "An Optical Study of Cathodic Hydrogen Evolution in High-Rate Electrolysis", J. Electrochem. Soc., Vol.117, No.6, P.840, (1970).
- (11) F.Hine, M.Yasuda, R.Nakamura, and T.Noda, "Hydrodynamic Studies of Bubble Effects on the IR-Drops in a Vertical Rectangular Cell", J. Electrochem. Soc., Vol.122, No.9, p.1185-1190, (1975).
- (12) F.Hine, and K.Murakami, "Bubble Effects on the Solution IR-Drop in a Vertical Electrolyzer Under Free and Force Convection Flow Conditions", J. Electrochem. Soc., Vol.127, No.2, P.292-297, (1980).
- (13) Ronald Alan Putt, "Studies of the Events Occuring at Gas-evolving Electrodes", M.S.Thesis, University of California, Berkeley, October 1975.
- (14) A.T.Kuhn, J.Bin Yusof, P.Hogan, "The Role of Electrode Structure and Surface Texture in the Performance of gas Evolving Electrodes", J. of Applied Electrochemistry, Vol.9, P.765-775, (1979).
- (15) C.W.Tobias, "Effect of Gas Evolution on Current Distribution and Ohmic Resistance in Electrolyte", J. Electrochem. Soc., Vol.106, No.9, P.833-838, (1959).

- (16) Kenneth G. Hellyar, "Cinematic Studies of the Anodic Dissolution of Metals at High Current Densities", M.S.Thesis, University of California, Berkeley, Sept. 1971.
- (17) J.Newman, "Electrochemical Systems", P.117, Prentice-Hall, Inc., Englewood Cliffs, N.J., 1973.
- (18) J.Newman, J. Electrochem. Soc., Vol.117, No.4, P.507-508, (1970).
- (19) L.I.Krishtalik, "Advances in Electrochemistry and Electrochemical Engineering", edited by P.Delahay and C.W.Tobias, Vol. 7, P.315, (1970).
- (20) Carl Wagner, J. Electrochem. Soc., Vol.98, No.3, P.121, (1951).
- (21) H.B.Clark, P.S.Streng, & J.W.Westwater, Chem. Engin. Prog. Symp. Ser., Vol.55, P.103 (1959).
- (22) Y.Y.Hsu, Trans. ASME, Ser. C, J. Heat Transfer, Vol.84, P.207, (1962).
- (23) Paul Sides, Ph.D. Thesis, University of California, Berkeley, Chem. Engin. Dept., 1980.